INFORMATION TO USERS

An Experimental Investigation of a
Solar Chimney Natural Ventilation System

Scott Spencer

A Thesis

in

The Department

of

Building, Civil and Environmental Engineering

Presented in Partial Fulfillment of the Requirements
for the Degree of Master of Applied Science at
Concordia University
Montreal, Quebec, Canada

March 2001

Canada

ii

ABSTRACT

An Experimental Investigation of a

Solar Chimney Natural Ventilation System

Scott Spencer

Natural ventilation driven by a solar chimney attached to a single-room building was studied experimentally using a small-scale model. The experiments were performed using a recently developed fine-bubble technique in which fine hydrogen bubbles are produced electrolytically in salt solution to simulate the buoyancy effect in the chimney caused by temperature differences.

During the experiments, one sidewall of the solar chimney was uniformly "heated", corresponding to a uniformly distributed solar radiation incidence. Velocities at the room inlet were measured by a particle tracking method; in turn, the average flow rate through the solar chimney system was determined. Parameters studied in the experiments were the cavity width of the solar chimney, the solar radiation intensity, the ventilation inlet areas, and the solar chimney height.

Results showed that for a given building geometry and inlet areas, there is an optimum cavity width at which maximum ventilation flow rate can be achieved. This optimum cavity width, which is independent of the solar radiation intensity, was found to be dependent on the size of the ventilation inlet areas and the solar chimney height. Observations were made on the flow patterns within both the solar chimney and the room.

Two simple theoretical models were developed, based on common tools found in literature used for solar chimney ventilation prediction. Comparison between the measured ventilation flow rates and the theoretical predictions indicated that theoretical models, based on simplified temperature assumptions within the chimney, may over-predict the solar chimney ventilation performance and should be used with care.

ACKNOWLEDGMENTS

TABLE OF CONTENTS

LIST OF FIGURES

LIST OF TABLES

NOMENCLATURE

Symbol	Meaning	Units
A	cross-sectional area	[m^2]
$A^{\bullet}$	effective opening area of the system	[m^2]
A_b	horizontal cross-sectional area of the boundary layer	[m^2]
b	boundary layer thickness	[m]
B	buoyancy flux	[cm^4/s^3]
c	local discharge coefficient	[-]
C_d	total discharge coefficient for the system	[-]
C_p	specific heat	[J/kg·K]
d	distance	[m]
D_m	diffusivity of the fluid from the buoyancy source to the ambient fluid	[m^2/s]
D_H	hydraulic diameter	[m]
D_T	thermal diffusivity of the ambient air	[m^2/s]
f	friction factor	[-]
g	acceleration due to gravity	[m/s^2]
g'	reduced gravity	[m/s^2]
h	height	[m]
h	heat transfer coefficient	[W/m^2·K]
H	total height of the solar chimney	[m]
k	thermal conductivity	[W/m·K]

k	loss coefficient	[-]
k_f	channel loss coefficient	[-]
L	characteristic length	[m]
$\dot{m}$	mass flow rate	[kg/s]
P	pressure	[N/m^2]
q	heat flow from source	[W]
q_h	heat flow per unit height	[W/m]
Q	ventilation flow rate	[m^3/s]
Q_1	ventilation flow rate predicted by Model 1	[m^3/s]
Q_2	ventilation flow rate predicted by Model 2	[m^3/s]
t	time	[s]
T	temperature	[K]
T_{fo}	temperature of fluid at the chimney outlet	[K]
u	fluid velocity	[m/s]
u_{ave}	mean fluid velocity	[m/s]
V	volume	[m^3]
w	width	[m]

Greek Symbols

α	angle relative to the horizontal	[°]
β	coefficient of thermal expansion	[1/K]
β_c	volume expansion coefficient due to concentration changes	[-]
ε	absolute roughness factor	[mm]

φ	concentration of liquid	[-]
ρ	density	[kg/m^3]
v	kinematic viscosity	[m^2/s]
θ	characteristic time scale	[s]

Subscripts

ci	chimney inlet
co	chimney outlet
g	gas (hydrogen)
h	height
i	inside chimney
L	losses
M	model
o	outside chimney
PT	prototype
ri	room inlet
s	salt-water
sc	solar chimney cavity
S	stack effect
W	wind

CHAPTER 1

INTRODUCTION

1.1 Natural Ventilation

Building ventilation is the intentional movement of air through a space so as to provide acceptable indoor air quality and, at times, to regulate thermal comfort. Ventilation may be forced or natural. Forced ventilation uses mechanical means, such as fans, to drive air through a building. On the other hand, natural ventilation makes use of natural forces such as density differences due to temperature (also known as buoyancy or stack effect) and wind to induce airflow.

Compared to mechanically ventilated buildings, naturally ventilated buildings use much less energy because of the reduced electricity needed for fans. A naturally ventilated building maintains adequate indoor air quality by drawing in ambient air, which is generally less contaminated than the indoor air, thereby eliminating the need for filtration processes.

Thermal conditions in a naturally ventilated building can be controlled to a certain extent by using natural ventilation in combination with underground plenums, water features, solar collectors, night cooling etc. Again, this can save considerable energy by reducing chiller and boiler usage. With the increasing awareness of the need to reduce greenhouse gas emissions and the need to develop effective, cost-efficient and ecologically sound building ventilation, natural ventilation techniques have become more attractive in recent years. In this work, one of the major items used for natural ventilation,

the solar chimney, which induces air through a building by utilizing renewable solar
energy, is investigated.

1.2 The Principle of Solar Chimney Ventilation

A solar chimney is a tall cavity, commonly positioned on the sunny side of a
building, as shown in Figure 1.1. The air within the chimney is heated by solar radiation,
giving rise to buoyancy forces, which drive the air upwards and out the solar chimney.
From mass balance, air exhausted from the chimney induces fresh outdoor air into the
building, through openings such as doors and windows, thereby providing ventilation to
the building.

2. Warm walls heat the air within the chimney, creating buoyancy forces that exhaust the air from the chimney.

Room

Outdoors

Solar chimney

1. Sun heats solar chimney walls.

Chimney inlet

Room inlet

3. Air exhausted from the chimney induces fresh air into the room inlet and provides ventilation.
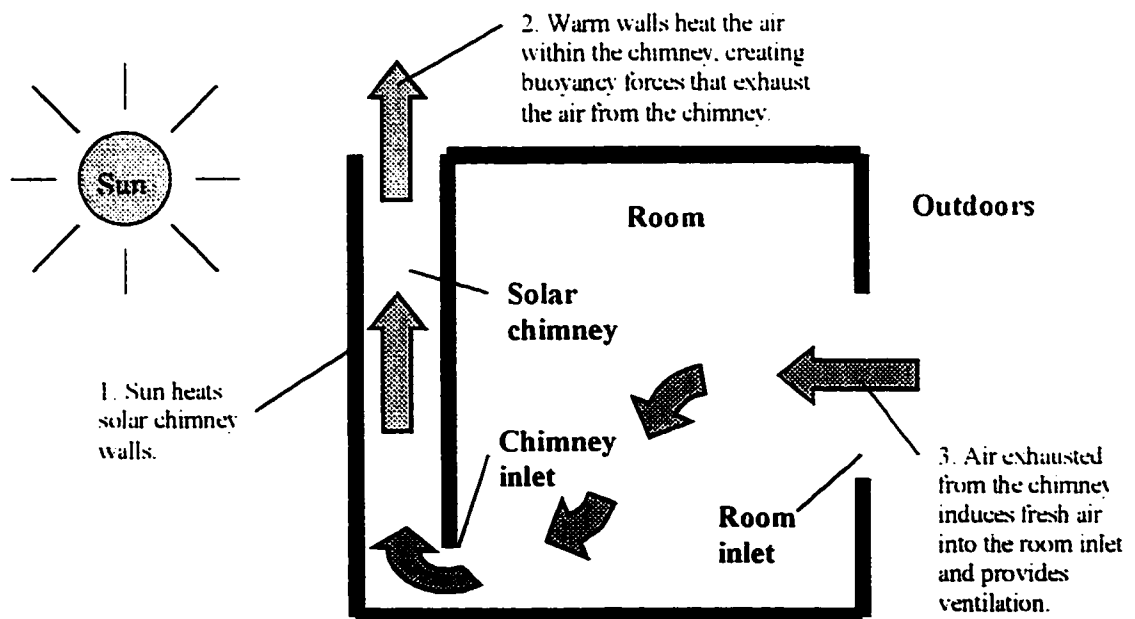
Figure 1.1 Operation of a solar chimney naturally ventilated building.

The principle of solar chimney ventilation is primarily based on stack effect, and depends on parameters such as the height of the solar chimney; the temperature difference between the air within the chimney and the outdoors; and the design and location of ventilation inlets. Theoretically, maximum flow rate through a solar chimney ventilated building may be achieved through a combination of increasing chimney height, temperature difference and ventilation opening areas. Wind, when present, can also assist to drive air through a solar chimney. A cap on the top of the chimney, for example, can enhance chimney operation by providing suction as wind passes over it, thereby drawing air out of the chimney. However, in the present work, wind effects are not considered for simplicity. It should be noted that a no-wind situation in a solar chimney ventilation system represents a worst-case scenario and any design based on this will be conservative.

1.3 Solar Chimney Configurations

Solar chimney ventilation is not new and has been used for hundreds of years. Solar chimneys can be found in historical buildings, such as the Sicilian villa "Scirocco rooms", dating back to sixteenth-century (Figure 1.2) where they were used in conjunction with underground corridors and water features to provide cooling [1]. The conical structure above the Scirocco room (Figure 1.2) acted as a solar chimney by increasing the air temperature within, thereby creating a stack effect. Consequently, airflow was induced, which was cooled in the underground corridor and water stream before refreshing occupants within the Scirocco room.

3

There are numerous varieties of ventilation devices given the name of solar

chimney, and they all operate on the same principle. A solar chimney for use in hot arid

climates may be similar to the one shown in Figure 1.3. In this case, the solar chimney

walls are made from a high thermal capacity material, allowing a nighttime ventilation

strategy to cool occupants within the building. During the daytime, dampers at the

entrance and exit of the chimney are closed, allowing the chimney walls to store heat. At

night, when the outdoor air is cool, the dampers are opened, and the stored heat in the

walls is transferred to the air within the chimney, thereby creating a temperature

difference between the chimney air and the outdoors, and a consequent movement of cool

air through the building.
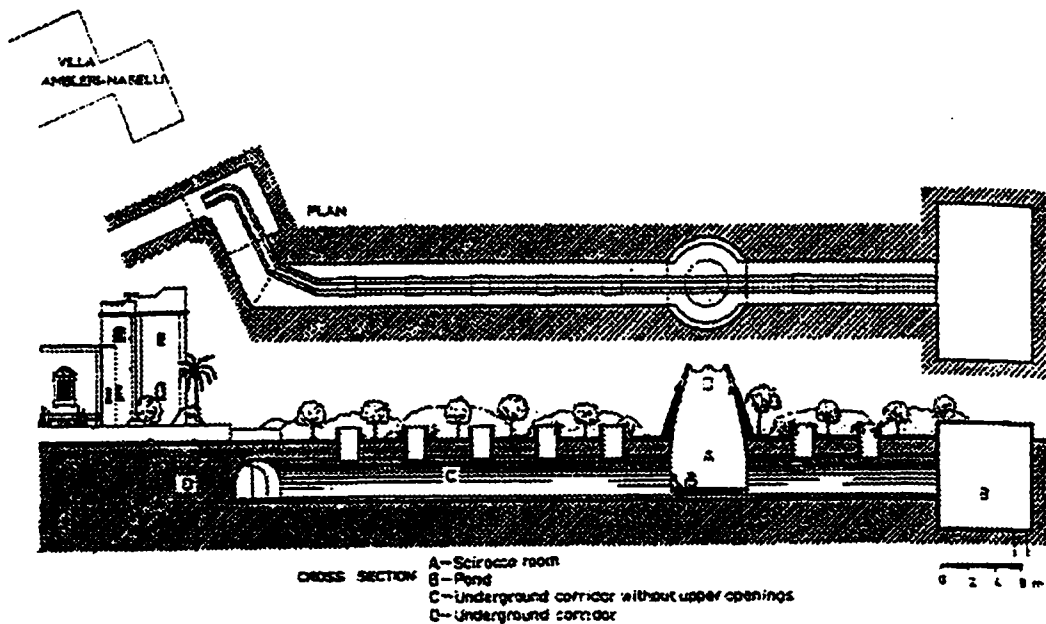
Figure 1.2 Plan and section of the ancient underground cooling system of the

Villa Ambleri-Naselli (from Di Cristofalo *et al* [1]).

A solar chimney may be incorporated into the roof of a building. such as the one shown in Figure 1.4. A chimney vent is provided at the side of the solar chimney. allowing the exhaust of air. In this instance, the solar chimney is made of corrugated metal, which has low thermal storage capacity, allowing ventilation to begin as soon as the sun adequately heats the metal. Therefore, this system is best suited to daytime ventilation, it having inadequate thermal capacity to maintain ventilation at night.
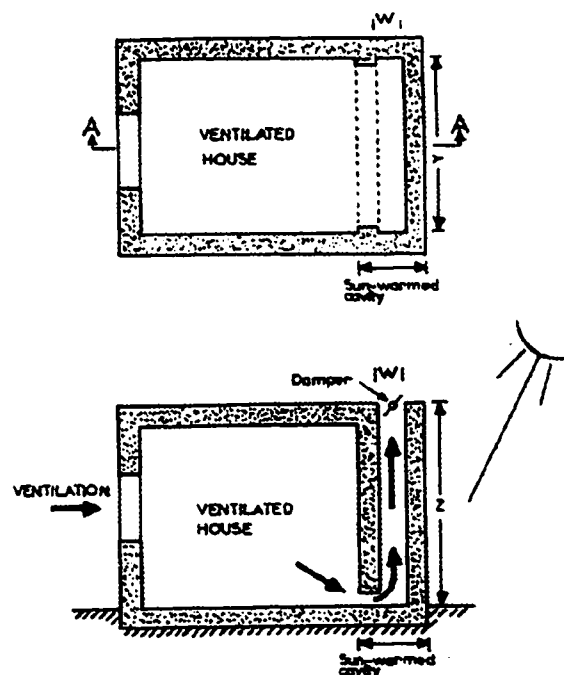
Figure 1.3 Solar chimney with high thermal storage capacity used for night cooling in hot arid climates (from Bouchair [2]).

Another example of a solar chimney incorporated into the roof of a building is shown in Figure 1.5. A glazed solar collector, installed on the sloping roof, heats air before it rises into the chimney. The advantage of this system is that the solar collector

helps in increasing solar heat gains and the slope of the roof can be designed to capture

maximum solar radiation.
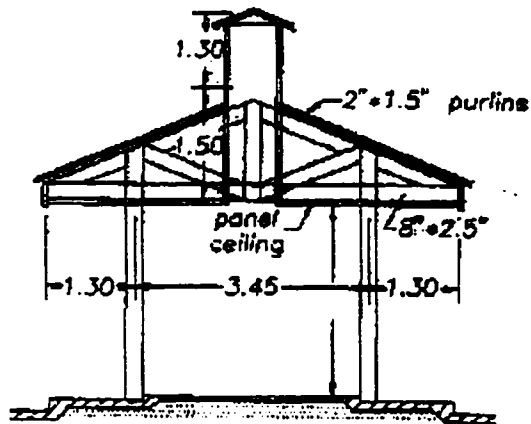
Figure 1.4 Solar chimney incorporated into the roof of a building for day cooling

(from Barozzi *et al* [3])
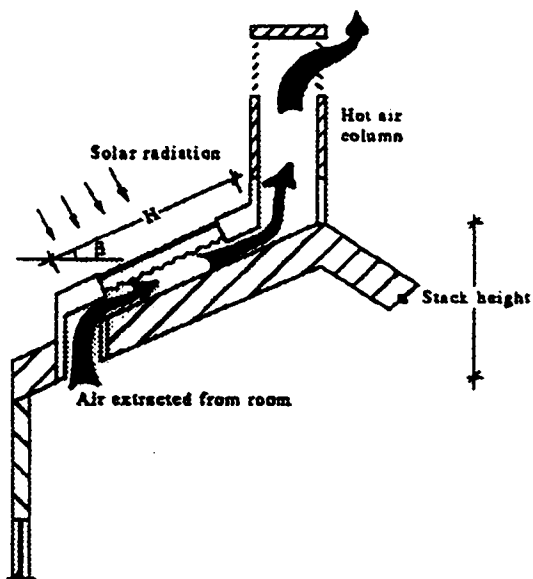
Figure 1.5 Solar chimney with sloping solar collector (from Bansal *et al* [4]).

Bansal *et al* [5] proposed a combined wind tower-solar chimney system. shown in Figure 1.6 In this system. wind induced ventilation is assisted by stack effect provided by multiple solar chimneys installed at the room outlets.
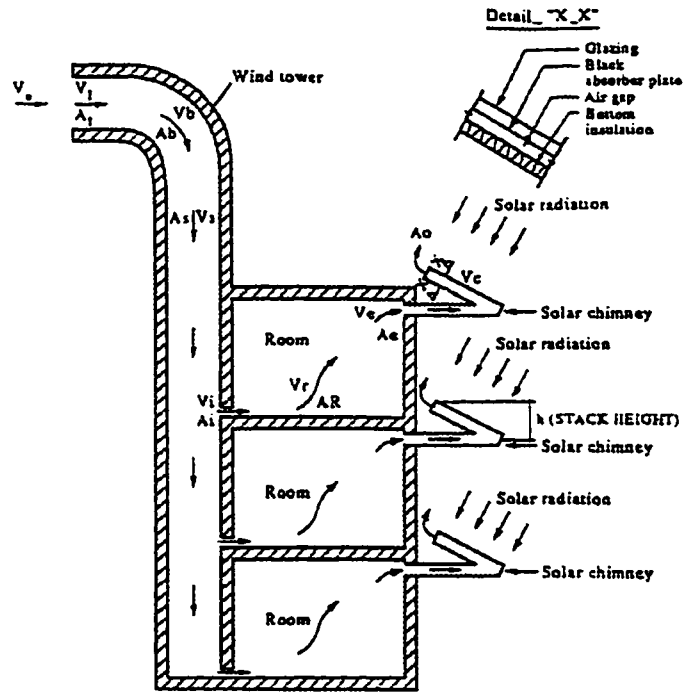
Figure 1.6 A combined wind tower – solar chimney building

(from Bansal *et al* [5]).

A system similar to the solar chimney is the Trombe wall (Fig. 1.7). Like the solar chimney, the Trombe wall consists of a cavity positioned on the sunny side of the building. The outer wall is usually glazed and the inner wall made of a material with high thermal capacity. However, unlike the solar chimney, extra openings exist in the inner and outer walls. and dampers are provided at all the openings for airflow control. The extra dampers and openings are used for different operation modes, such as heating and

cooling. Trombe walls can also ventilate as a solar chimney, simply by opening the bottom inner wall and the top outer wall vents, as shown in Fig. 1.7 (b). However, the solar chimney is more effective than the Trombe wall for ventilation purposes because extra pressure losses in the Trombe wall system (due to additional elbows and dampers) limit the amount of air that can flow through the system [6].
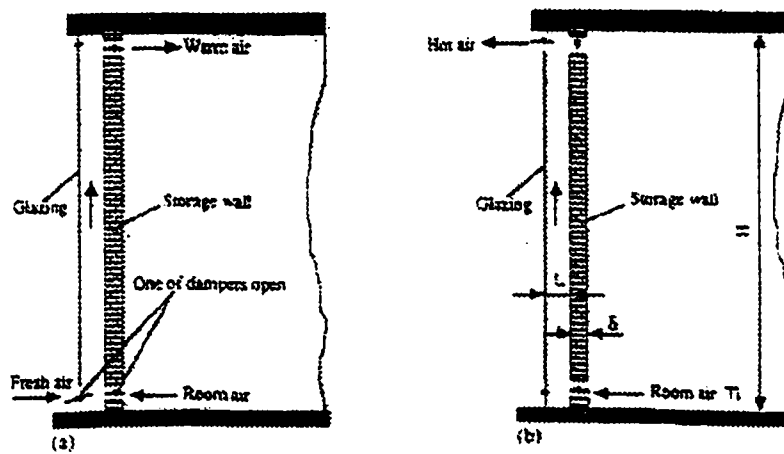
Figure 1.7 Schematic of a Trombe wall system for (a) winter heating and (b) summer cooling (from Gan [6]).

There are various other forms of solar chimneys that are not mentioned in this section, however their basic operating principle is the same. Different geometries and materials are at the designer's disposal and should be used according to site conditions and the mode of operation required, be it daytime ventilation, nighttime ventilation or cooling.

1.4 Layout of the Thesis

This thesis is divided into six chapters. A literature review of important works pertaining to solar chimney research is detailed in Chapter 2. This review considers mainly experiential and analytical research, as they are the methods of investigation used in the present work. In addition, useful information from some computational works is presented. Stemming from the literature review, the objectives of the present work are described.

Details of the experimental set-up and apparatus used are described in Chapter 3. Additionally, the experimental method, a fine-bubble technique, is described, as is the similarity requirements and scale-up criteria.

The results of the experiments, including an uncertainty analysis, are presented and discussed in Chapter 4.

In Chapter 5, two simple analytical models are developed. The analytical models are compared to the experimental results and discussed.

Conclusions based on the present work and pointers to areas for further research are contained in Chapter 6.

CHAPTER 2

LITERATURE REVIEW AND OBJECTIVE

Although the solar chimney ventilation technique has been used in buildings for hundreds of years, airflow in a solar chimney and its ventilation performance are still not well understood. For example, solar chimney designs rely mainly on experience and there is no standard prediction tool for ventilation flow rate for a solar chimney. In the recent two decades, due to the increasing need for utilizing renewable energy, a number of investigations in solar chimneys have been carried out.

The main research techniques used in solar chimney ventilation are experimental, analytical and computational. In this chapter, a literature review is carried out on solar chimneys, Trombe walls and other solar collectors, with similar geometries and operating principles, in order to gain the current understanding in this field.

2.1 Review of Experimental Works

An important research technique for airflow in buildings is experimental modeling. Experimental modeling provides the opportunity for creating and observing realistic fluid flow in controlled conditions. Analytical and computational models often need to be validated against experimental data before they can be confidently applied in reality. Additionally, experimental modeling allows investigation of complicated geometries, which may be far beyond the scope of computer modeling [7]. However, experimental modeling can be expensive and desirable boundary conditions are not always attainable.

In most building applications. experimental modeling can be divided into two classifications, based on model size: full-scale modeling and small-scale modeling. Using a full-scale model has the advantage over a small-scale model in that it is unnecessary to invoke scaling laws in order to attain similarity between the model and the prototype – behaviors observed in the model will be the same as those observed in reality, as long as conditions are the same. However, using a full-scale model is certainly not always practical. Scale models tend to be less expensive and are sometimes necessary in order to study certain aspects of building design under controlled laboratory conditions [3].

Previous experimental research in solar chimney ventilation has contributed significantly to the understanding of solar chimney performance. although the number of these investigations is still quite limited. The most relevant investigations to the field of building ventilation are described below.

Bouchair [2] completed an important study of a solar chimney for cooling ventilation: Figure 1.3 shows a schematic view of the solar chimney system used. The chimney had a fixed height of 2m with both walls maintained at the same temperature The influence of chimney width, chimney inlet height (and thus inlet area) and surface temperature (T_{sm}) of both chimney walls was investigated.

Figure 2.1 shows the effect of chimney width on the mass flow rate for inlet heights of 0.1m and 0.4m with the chimney wall temperatures in the range of 30 to 60°C. The ambient air temperature was maintained constant at 20°C. It was found that in the chimney width range of 0.1m – 1.0m, there was an optimum chimney width between 0.2 and 0.3m, which gives maximum ventilation rate. It was also found that this optimum chimney gap is essentially independent on the chimney wall temperature. However, it

may be seen that the optimum gap is slightly wider when the chimney inlet becomes

higher from 0.1 m to 0.4m.
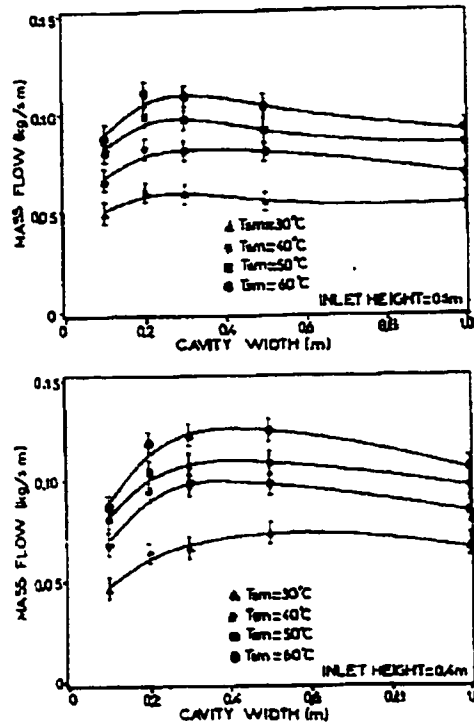
Figure 2.1 Effect of cavity width and inlet height on the airflow rate (from

Bouchair [2]).

In Bouchair's experiments, a mass balance investigation was also carried out for

the mass flow rate through the window (room inlet), the chimney inlet and the chimney

outlet. Continuity was found to exist at chimney widths of 0.1 m, 0.2m and 0.3m.

However, at a chimney width of 0.5m, the measured mass flow rate at the chimney outlet

was higher than that through the window and the chimney inlet. Smoke visualization

showed that at the chimney outlet the smoke traveled entirely upward for chimney widths

from 0.1 m to 0.3m. However, at a chimney width of 0.5m, there was reverse flow

downwards through the chimney in the central section The upward flow near each wall

was supplied partly by the air from the room inlet and partly from the air flowing

downwards through the outlet in the central section of the chimney (see Fig. 2.2). This

phenomenon explains the increased mass flow rate measured at the outlet and also

explains why the mass flow rate through the system decreased as the chimney was wider

than the optimum gap. When the boundary layers covered the whole chimney width. the

flow was entirely upward. However, as the chimney width was increased beyond the

coverage of the boundary layer, reverse flow could occur in the central section and this

resulted in a decrease in the mass flow rate.
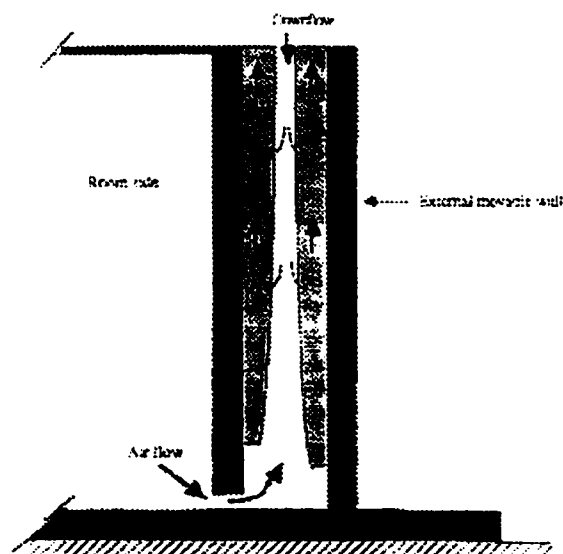
Figure 2.2 Possible flow pattern with back-draughting at large chimney widths

(from Bouchair [2]).

Smoke visualization showed no flow reversal through the window and the inlet. It

was also observed that air flowed through the window, along a streamline, to the chimney

13

inlet. There was almost no air movement in the building above and below the window. Consequently, it was suggested that the window should be positioned such that ventilation can affect most of the internal space.

Figure 2.3 shows the effect of the inlet height on the mass flow rate at two inlet heights: 0.1 m and 0.4m for the chimney width in the range of 0.1m to 0.5m. It is seen that at a chimney width of 0.1m, the mass flow rates were similar at both inlet heights. This suggests that the inlet height at this chimney width had little influence on the ventilation flow rate and the friction loss in the chimney dominated the total pressure loss in the system. However, it can be seen that with an increase in width, friction loss in the chimney was reduced and the influence of chimney inlet height became more and more significant. Consequently, the friction loss at the inlet became the major contribution to the total pressure loss and determined the mass flow rate through the whole system at the larger chimney widths.

From his experimental results, Bouchair concluded that the optimum chimney width was approximately one-tenth of the chimney height, or an aspect ratio (H/w) of 10.

Kumar *et al* [8] studied the indoor air quality in a solar chimney system. The prototype house consisted of a single chamber (7 × 11 × 3m) with a chimney (5m high, 0.5m in diameter and an effective inlet area of 0.1 m^2) located away from the house and surrounded by a green belt of Pulownia plantations. An underground tunnel connected the chimney to the house.

A total of four indoor air samples were collected for a 24-hour period and were taken at intervals of seven days for a month. It was concluded that passive outdoor air ventilation together with a green belt is effective in reducing indoor air contaminants.

14
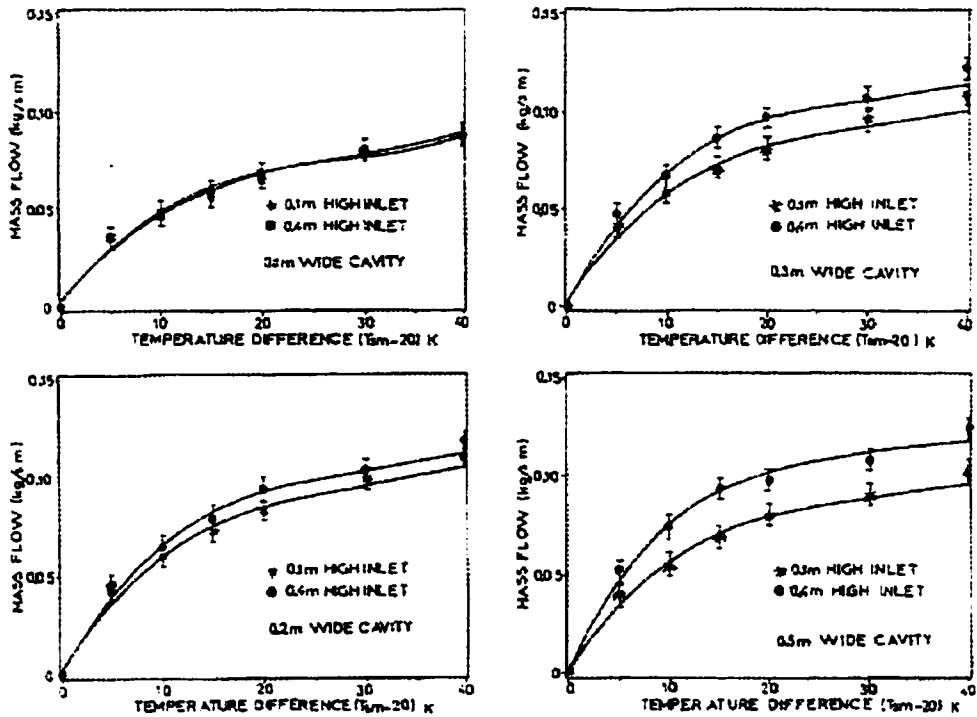
Figure 2.3 Effect of inlet height on airflow rate at various chimney widths (from Bouchair[2]).

Khedari *et al* [9] performed an experiment to investigate the effectiveness of a solar chimney ventilation system in reducing heat gains through natural ventilation in a house. The effect of door, window and solar chimney inlet openings on the ventilation rate was studied.

The full-scale study was performed in a single-room schoolhouse, approximately $25m^3$ in volume. Four different solar chimney configurations were used. Three types of solar chimneys were installed in the south-facing wall, each unit having an area of $2m^2$: the Trombe Wall, the Modified Trombe wall and the Metallic Solar Wall. On the

southern side of the roof two Roof Solar Collector units were installed. each having an area of 1.5m².

The experiments showed that natural ventilation, induced by the solar chimneys. reduced room overheating by about 50%, with the air change rate varying between 8-15. Thermal comfort was found to be unsatisfactory at the tested conditions because of low air velocities. It was suggested that increasing the surface area of the solar chimneys could increase air velocity.

Afonso and Oliveira [10] performed a full-scale experiment in which they compared the natural ventilation performance of a solar chimney and a conventional chimney. In this case, a solar chimney was defined to be similar to a conventional chimney except that the south wall was replaced by glazing. Additionally, a thermal model was developed for solar chimney simulation, taking into account both solar and wind effects. This model was validated by experimental results and was used to investigate other parameters (e.g. chimney wall thickness, effect of insulation, etc.).

The tests were performed in a test cell, with a floor area of 12m² (4 × 3 m). The test cell was divided into two identical test rooms, one with a solar chimney and one with a conventional chimney. Both exhaust chimneys had a cross section of 0.2 × 1m and a height of 2m. The walls, ceiling and slab of the test rooms were made of concrete with outside insulation. The chimneys were made of brick (10cm thick) with outside insulation (5cm thick) for the solar chimney. Inlet ducts were provided in the rooms through the roof (see Fig. 2.4).

The main aim of the experiment was to compare the conventional and glazed solar chimneys and use this data for their computer model validation. Experimental tests

were performed on two separate days. one with a period of high solar radiation and one with a period of low solar radiation. The only variables in the experiment were the outdoor ambient conditions on these two days, thus the experiment itself offered little information. However, it was found that the glazed solar chimney generally performed better than the conventional chimney. Improvements were more pronounced on the day of high solar radiation. with a 30% increase in air change rate per hour (ACH). while improvement was only marginal on the day of low solar radiation, with a 3.5% increase in ACH.
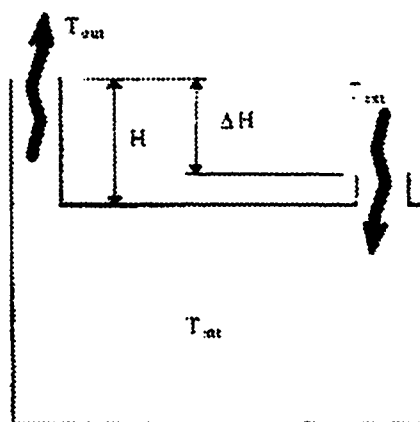
Figure 2.4 Schematic view of the solar chimney system considered (from Afonso and Oliveira [10]).

Sandberg and Moshfegh have undertaken a number of investigations in fluid flow and heat transfer in vertical channels heated on one side by PV elements. One experimental study [11] was performed in a laboratory using a rectangular channel, 1.64m (depth) × 0.23m (width) × 6.5m (height). An electrically powered heating foil was installed on the inside wall on one side to provide a uniform heat flux into the channel.

The outer perimeter of the channel was insulated to ensure that most of the heat generated entered the channel.

The airflow rate in the channel was measured using a tracer gas technique while the heat flux into the channel was varied from 25 – 300 W/m^2. Temperature was measured on the heated and unheated walls of the channel using thermocouples. Tests were carried out for two conditions at the channel exit at the top: firstly, with the channel top completely open; and secondly, with a rain protection cap installed at the top, which reduced the outlet area to only 4% of the open end area.

Results showed that the flow rate increased with increasing heat input and that the rain protection severely limited air flow through the system. The flow was entirely laminar for the channel with the rain screen but was transitional for open ends, that is the flow started off laminar but reached a stage of turbulence at some point along the height of the channel. It was calculated that approximately 40% of the total heat supply was absorbed by radiation on the unheated surface.

Sandberg and Moshfegh [12] made another similar investigation of a channel heated by a constant heat flux. Again, heating foils were used to heat air in the channel and the flow rate through the channel was measured using a tracer gas technique. Local velocities were measured using a thermistor anemometer and temperatures were measured.

Investigated, in this experiment, were the inclination angle of the channel, the position of the solar cell module (or heating foil) and the aspect ratio of the channel. Aspect ratio was investigated with a vertical channel 6.5m high and measurements were

18

taken at channel widths of 0.23, 0.115 and 0.06m. Inclination angle was investigated using a channel 5m high and 0.05m wide with angles varying from 20 to 90°.

Results showed that the velocity through the channel increased with aspect ratio, or the flow rate increased with increasing channel depth. An optimum flow rate, such as that found by Bouchair [2], was not indicated here. However, with the range of aspect ratios inspected it is not expected that the channel widths were wide enough for an optimum to occur, with an aspect ratio of 28 being the lowest in this study compared to Bouchair's aspect ratio of about 10.

The velocity profiles measured in this experiment suggest a complicated flow pattern in the channel; see Figure 2.5. Temperature profiles across the channel depth are shown in Figure 2.6 for numerous incline angles. Radiation heats the initially unheated wall, so there are higher temperatures near the walls, giving the profiles their "U" shape. It can be seen that there is significant temperature variation between the air at the wall surface and air in the middle of the channel. This again indicates a complicated flow pattern.

Moshfegh and Sandberg [13] carried out another numerical and experimental study on the airflow in gaps behind PV panels. They used the rig and the flow rate measurement technique as described in [11], for heat fluxes in the range $20 - 300 \text{W/m}^2$. They found temperature and velocity profiles in the gap at various heat fluxes and also investigated convective and radiative heat transfer from the wall to the air. It was found that, for a fixed input heat flux, the average velocity at the channel outlet decreased for surfaces with lower emmisivities.
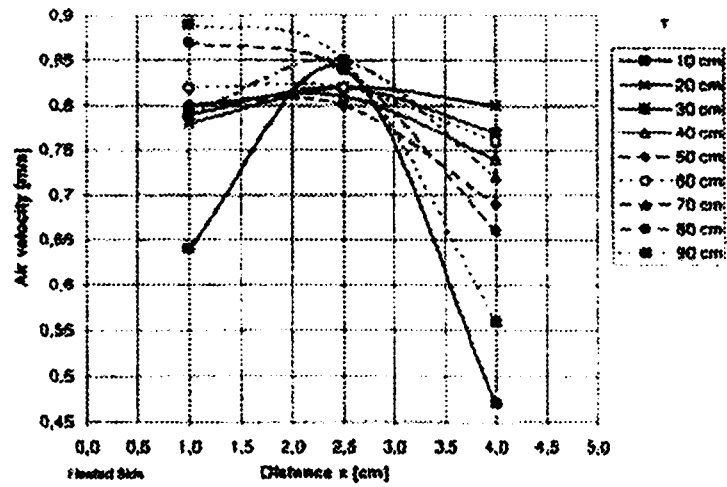
Figure 2.5 Velocity distribution in the vertical channel (from Sandberg and
Moshfegh [12]).
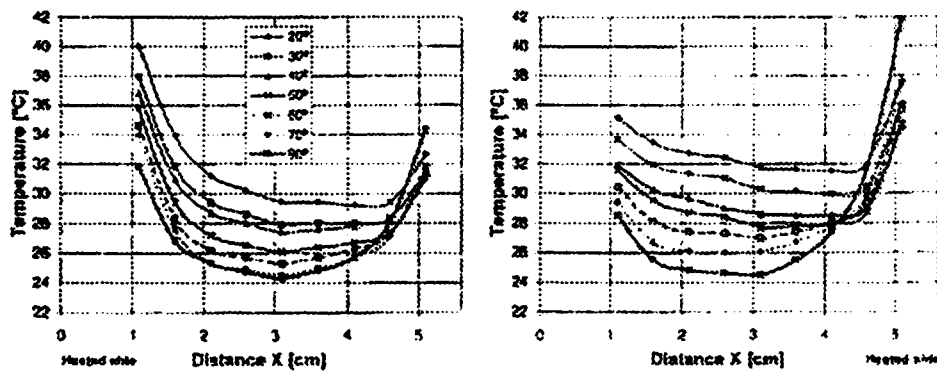
Figure 2.6 Air temperature profile as a function of inclination angle (from
Sandberg and Moshfegh [12]).

Swainson [14] completed a thorough investigation of a solar chimney ventilation

system. He compared basic mathematical and CFD models used to predict flow rate

through a solar chimney with experimental results obtained from his study.

A full-scale rig was used in the experiments. and was positioned outdoors. open to the natural environment. The rig was set up such that the solar chimney was shielded from wind and was therefore driven exclusively by stack effect. Thermocouples were used to measure temperatures on the solar chimney surfaces and a high precision thermistor was used to measure air velocity and temperature entering and exiting the solar chimney.

Experiments were used to investigate the following parameters: heat transferred from a single wall of a solar chimney, in the range 50 - 200 W/m². chimney inlet height. for 0.075 and 0.15m: chimney width: and chimney heights in the range 1.5 - 3.75m.

As expected, results showed that the mass flow rate through the chimney increased with chimney height, inlet height and with heat transferred from the chimney wall to the air within the chimney. When the chimney width was varied. an optimum flow rate was found to occur. as was indicated by Bouchair [2].

Additionally, the optimum chimney width was shown to increase as the chimney height increased. These results corresponded closely to the theoretically predicted turbulent boundary layer thickness established by Eckert and Jackson [15] (examined further in the next section). Calculations showed that the maximum mass flow rate occurred when the boundary layers just spanned the chimney width, confirming Bouchair's [2] findings.

Swainson [14] found that beyond the optimum channel depth, the mass flow rate was largely insensitive to increasing chimney depth at chimney heights above 2.25m. Results also indicated that, for a given height, the optimum width remained constant, independent of heat transfer from the plate.

Lane-Serff *et al* [7] undertook an experimental study of an Engineering School at Leicester Polytechnic, which utilizes a solar chimney natural ventilation system. The aim of the study was to assess the performance of the ventilation system in providing fresh air to the occupants, taking into account stack effect and internal heat gains

A brine-water system was used in the experimental investigation of a multi-zone, small-scale (1:75) model. The model was constructed of perspex to allow flow visualization. A range of ducts and vents were incorporated into each space to investigate the most effective ventilation strategy. The effect of a fire in one of the spaces was also investigated.

Experimental results indicated that the ventilation system was generally adequate in providing fresh air to the occupants. It was suggested that it would be better to have isolated systems with separate vents in each space rather than different spaces sharing the same vents. It was found that small differences in heat gains in one space could significantly affect the flow in an adjacent space sharing the same inlet vent, causing flow to be unpredictable. Isolated spaces have a more predictable and stable flow and are also better for fire and smoke containment.

Barozzi *et al* [3] carried out an experimental and numerical study of a building with a solar chimney to assess the thermal performance of an existing prototype in Nigeria, see Figure 1.4. The experiment was performed using a small-scale model and the results were used to validate a two-dimensional, CFD simulation model.

The experimental building prototype in Nigeria consisted of a single chamber, approximately 5.5m (length) × 3.5m (width) × 3.0m (height), with a corrugated metal roof and a fiberboard ceiling. A solar chimney was built into the roof to provide

ventilation and cooling. Air flowed in through the windows and was exhausted out through the top of the solar chimney. Different window arrangements were obtained by maneuvering the light wooden wall panels, thus allowing the effect of different geometries on the airflow to be examined. The experiment was performed with a 1:12 scale model of the prototype, constructed with the same materials where possible. Figure 2.7 depicts the model form and construction details.
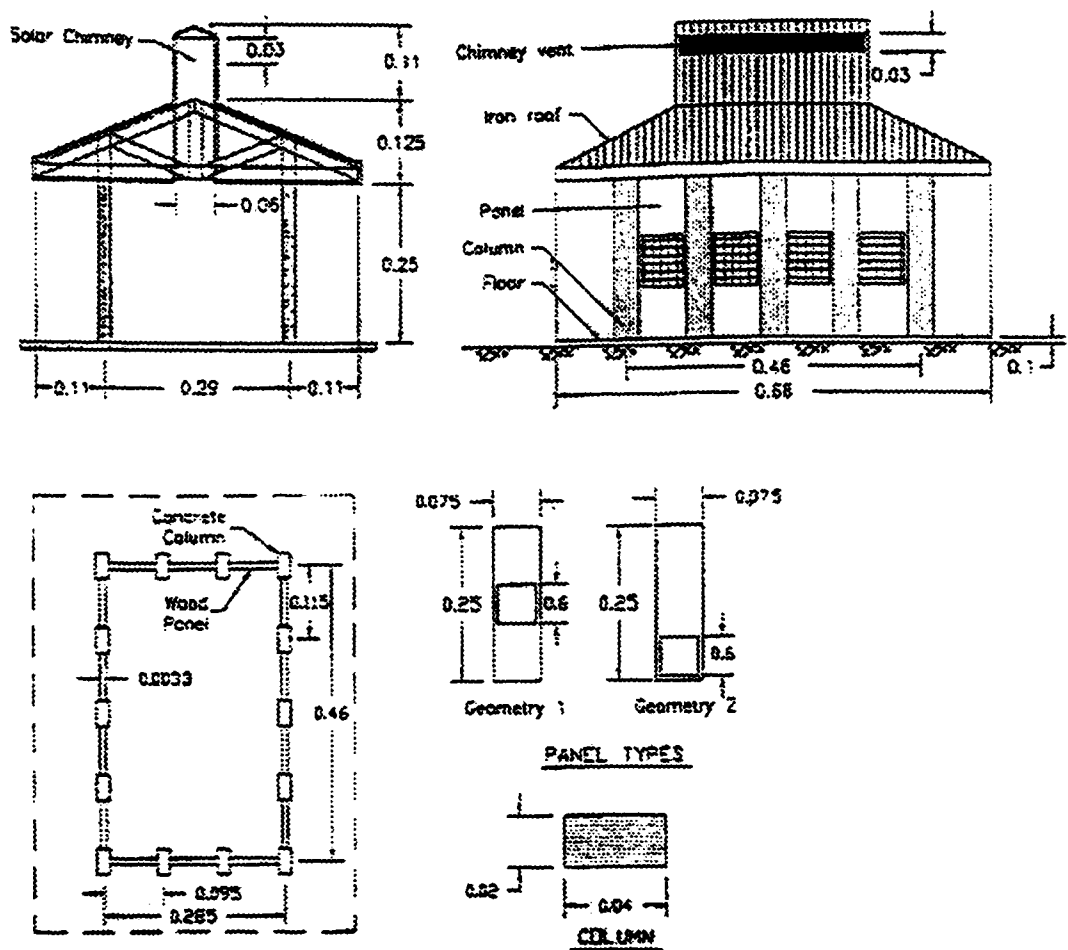
Figure 2.7 Model building details and dimensions (from Barozzi [3]).

The experiment was performed in a sealed laboratory chamber for the conditions of overhead sun and no wind, the scenario placing highest demand upon the ventilation system. Climatic parameters were limited to the ambient outdoor temperature and solar radiation. Relative humidity was assumed to be constant. Several series of tests were taken to assess the reliability and repeatability of their experimental data.

A simple solar simulator consisting of four Osram Ultra-Vitalux lamps were placed above the model to heat its roof. Once steady-state conditions were achieved, a PC data acquisition system recorded converted data from temperature and velocity sensors. Velocity measurements were limited to the solar chimney outlet region as velocities at other sections were too low to allow accurate measurement. Their air velocity measurements were estimated to have an accuracy of $\pm$ 20% in the experimental range of 5-50 cm/s.

Flow visualization was achieved by injecting smoke near the inlet (window) and recording the smoke trails on film.

For the numerical simulation, the following simplifications were made in their work:

- The problem was two-dimensional
- Radiation, inside the building, was negligible
- Flow was steady and laminar.

Results from numerical and experimental model were generally in good agreement, although the numerical model tended to over-predict the level of thermal stratification near the chimney exit region.

The results showed that the flow pattern in the room was very sensitive to the window geometry: for geometry #1, the air flowed in directly along a path from the window inlet to the ceiling opening; while for geometry #2, the air flowed from the inlet, almost vertically along the wall to the ceiling and then through the ceiling opening. Air velocities inside the building were found to be generally very low suggesting that the cooling effect may be less than required. Large flow velocities were predicted along the inclined roof surfaces due to high buoyancy forces.

2.2 Review of Analytical Works

Most of the analytical studies encountered in literature describe a simple, steady-state model to predict the ventilation flow rate, Q, through a solar chimney. It is the familiar orifice equation determined from the Continuity and Bernoulli's equation, with the following general form:

$$Q = A^* \sqrt{\frac{2\Delta P}{\rho}}$$

(2.1)

where ρ is a reference density and A^* is the effective area, which depends on the amount of openings, their cross-sectional area, their placement relative to one another (i.e. in series or in parallel) and their corresponding pressure losses. The driving pressure, ΔP, in a naturally ventilated building is the sum of the driving pressures of wind (ΔP_W) and stack effect (ΔP_S), i.e.

$$\Delta P = \Delta P_W + \Delta P_S$$

(2.2)

Considering only stack effect

25

$$\Delta P_b = \int_{-b}^{b} (\rho_o - \rho_i) g \, dh \tag{2.3}$$

where H is the height of the chimney channel, ρ_o is the density of the outside air, and ρ_i is the density of the air in the chimney. Commonly, ρ_i is assumed to be constant within the chimney or to vary linearly with height. Equation (2.1) may also be put in terms of temperature:

$$Q = A^* \sqrt{\frac{2\Delta Tgh}{T}} \tag{2.4}$$

Studies concerning an analytical analysis of solar chimney ventilation are reviewed below.

Bansal *et al* [4] developed a steady-state mathematical model for a solar chimney. Figure 1.5, shows a typical system to which the model can be applied. The system was comprised of a solar collector on top of a roof, which heats the air from the room and forces it upwards out the chimney.

Combining the Bernoulli and Continuity Equations, the volume flow rate can be expressed as

$$Q = C_d A_{co} [1 + (A_{co} / A_{ci})^2]^{-1/2} [2(\Delta T / T) gH \sin \alpha]^{1/2} \tag{2.5}$$

where the subscripts *co* and *ci* represent the chimney outlet and inlet respectively, and α is the angle of the collector relative to the horizontal. This takes the form of the Equation (2.4) above, where the inverse square-root term multiplied by $C_d A_{co}$ represents the effective area. In this study, discharge coefficients of 0.5, 0.6, 0.7, and 0.8 were considered. However, in this case, the equation is based on the difference between the temperature at the inlet and outlet of the chimney, as opposed to the difference in

26

temperature between the inside and outside of the chimney. The height is multiplied by $\sin\alpha$ to take into account the slope of the collector.

Air temperature of fluid exiting the outlet (T_{fo}), to be used in the Equation (2.5), was derived from an energy balance between the absorber plate and the air in the collector:

$$T = A(t) - B(t)\exp(-CL) \qquad\qquad (2.6)$$

where $A(t)$ and $B(t)$ are time dependant parameters, C is a constant and L is the length of the collector.

Unfortunately, no computational or experimental results were presented to confirm the validity of this model.

Bansal *et al* [5] also performed an analytical study for a solar chimney assisted wind tower system. The system proposed (see Figure 1.6) utilizes a wind tower to catch wind and direct it downwards through the rooms with the aid of solar chimneys located at the exhausts. Their treatment of the problem was similar to that in [4] but with adjustments for wind and the differing geometry. Again, no experimental or numerical results were presented to validate the results.

A mathematical model was developed by Hamdy and Fikry [16] to determine the optimum tilt angle for a solar chimney system at a specified region of 32° north latitude. Bansal *et al* [4] specified the solar chimney system under consideration (see Fig. 1.5). The author used Equation (2.5) of Bansal *et al* [4] and the concept of solar heat gain factor, *SHGF*, to determine the optimum tilt angle for a south orientated solar collector for best performance during the summer months. A tilt angle of 60 degrees to the horizontal was found to be the optimum for the studied zone.

27

Awbi [17] presented general design parameters and procedures for calculating the airflow rate, due to wind and buoyancy, in natural ventilation systems, namely solar chimneys, Trombe walls and roof collectors.

The equation for airflow due to stack effect takes the same form as Equation (2.4) and takes into account pressure losses at the ventilation openings and friction losses in the chimney. The temperature of the air exiting the chimney (T_{fo}) was found by an energy balance in the chimney assuming constant wall temperature:

$$T_{fo} = \frac{A}{B} + \left(T_i - \frac{A}{B}\right)e^{\left(-\frac{B*H}{\rho^*{}_p Q}\right)}$$ (2.7)

where $A = h_1 T_{w1} + h_2 T_{w2}$ and $B = h_1 + h_2$, T_w is the wall temperature, h is the heat transfer coefficient, subscripts 1 and 2 represent the two walls and H is the height of the chimney.

Model predictions were compared to the experimental results of Bouchair [2] and are shown in Figure 2.8. The results show fairly good correlation between the experimental and theoretical results; it does not predict an optimum cavity width however (as discussed above, Bouchair[2]) which occurred at about $w = 0.2m$.

It was concluded that solar-induced natural ventilation systems could provide adequate ventilation for moderate thermal and pollution loads. However, for large loads, solar ventilation systems may have to utilize wind pressure or be coupled with a mechanical system to provide adequate ventilation.

Padki and Sherif [18] developed a simple analytical model for a solar chimney to be used for electric power generation. In their study they found expressions for mass flow rate, the power generated and the efficiency of the chimney via simplified governing

equations of continuity. momentum and energy. The following expression was found for

the mass flow rate, $\dot{m}$, through the chimney:

$$\dot{m} = \rho_a A (2gh \, \Delta T_i T_a)^{1/2} / (T_a + \Delta T)$$

(2.8)

where T_a is the temperature of the ambient and $(T_a + \Delta T_i)$ the temperature in the chimney
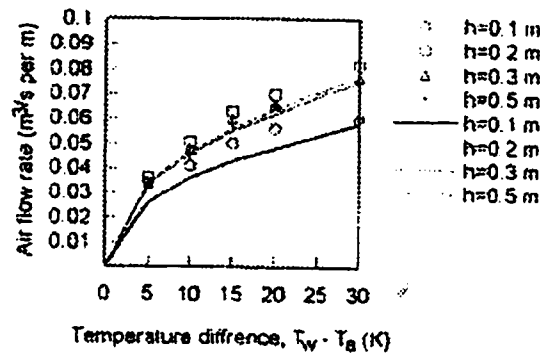
Figure 2.8 Comparison of Awbi's calculated airflow rate (shown with lines) with

Bouchair's experimental results (shown with symbols) for various chimney widths (h)

(from Awbi [17]).

Bouchair [19] used expressions found by Eckert and Jackson [15] to predict the

boundary layer thickness and mass flow rate of air in the boundary layer along the solar

chimney walls. Eckert and Jackson give the following expression for turbulent boundary

layer thickness from a vertical flat plate:

$$b = 0.565Gr^{1/10} Pr^{8/15} (1 + 0.494Pr^{2/3})^{1/10} h$$

(2.9)

With $Pr = 0.7$ (for air) and a temperature difference of 20 K between the chimney walls

and the ambient, Equation (2.9) simplifies to

$$b = 0.08h^{0.7}$$

(2.10)

Therefore, at a chimney height of $h = 1.95$m, $b = 0.128$m. This is in agreement with the experimental results, where the boundary layer thickness from each wall was found to be about 0.125m, i.e. one half of the optimum chimney width. This comparison was done for a chimney inlet height of 0.1 m, but for a chimney inlet height of 0.4m the optimum chimney width increased significantly; a factor not mentioned by Bouchair [19].

Eckert and Jackson gave the velocity distribution across the boundary layer (u_x) by the semi-empirical relation

$$u_x = C\left(\frac{x}{b}\right)^{1/7}\left(1 - \frac{x}{b}\right)^4 \tag{2.11}$$

where

$$C = 1.85(\gamma/H)Gr^{0.5}(1 + 0.5Pr^{2/3})^{-0.5}$$

$$\gamma = 1.5 \times 10^{-5}$$

and x is in the horizontal coordinate perpendicular to the wall.

Bouchair [19] integrated this expression over the boundary layer thickness to obtain the mean velocity (u_{ave}) in the boundary layer:

$$u_{ave} = 0.15C \tag{2.12}$$

The volumetric flow rate in the boundary layer is then

$$Q = u_{ave}A_b \tag{2.13}$$

where A_b is the horizontal cross-section of the boundary layer. Such an expression is a departure from the traditional, purely analytical method for determining the flow rate through a solar chimney outlined by Equation (2.1). Equation (2.13) of course applies only within the boundary layer. For two walls separated by $2b$, the volumetric flow rate will be doubled.

The measured results for an inlet height of 0.1m were found to be slightly lower than those predicted by Equation (2.13), apparently due to increased pressure losses at the inlet. Whereas the measured results for a cavity inlet height of 0.4m were found to be somewhat higher than those predicted, due to decreased pressure losses at the inlet. However, Equation (2.13) was generally found to be in good agreement with the measured results. Both comparisons were done at a cavity width of 0.3m.

2.3 Review of Computation Works

Afonso and Oliveira [10] presented the following simple expression to predict the ventilation flow rate through the chimney and incorporated it into their computation model:

$$Q = \frac{1}{\sqrt{k_{ci}\left(\frac{A_{co}}{A_{ci}}\right)^2 + k_{co} + f\frac{H}{D_H}}} A_{co} \sqrt{2\beta g \Delta T \Delta H} \qquad (2.14)$$

where A_{co} and A_{ci} are the area of the chimney inlet and outlet, respectively; f is the friction factor; D_H is the hydraulic diameter; H is the height of the chimney; k is the pressure loss coefficient; and β is the coefficient of thermal expansion. As can be seen, this equation takes the form of Equation (2.4), where the inverse square root term multiplied by A_{co} represents the effective area, A^*.

The computational model was insufficient in predicting the ventilation flow rate due to the presence of wind and had to be adjusted accordingly. There was better correlation between experimental and computational results once wind effects were taken into account.

Gan and Riffat [20] carried out a steady-state, turbulence model CFD simulation to examine a glazed solar chimney for heat recovery in a naturally ventilated building. A large amount of heat is exhausted from naturally ventilated buildings, solar chimney systems inclusive, thus the aim of their study was to use a CFD program to investigate the airflow and heat transfer in a solar chimney with heat-pipe heat recovery.

It was pointed out that a one-dimensional flow model would not be able to predict backdraughting in the solar chimney simulation. The reason for this is that the driving pressure term will always be positive as long as the average temperature in the chimney is greater than that outdoors. Consequently, the predicted flow in the chimney will be entirely upwards. Equation (2.15) below shows Equation (2.3) in terms of temperature:

$$\Delta P = gH \frac{\rho}{\beta} \left(\frac{1}{T_o} - \frac{1}{T_h} \right)$$

(2.15)

where β is the coefficient of thermal expansion, T_o is the outside temperature and T_h is the mean temperature of the chimney at height h. Equation (2.17) is not appropriate if reverse flow exists in the chimney and a multi-dimensional CFD technique should be used.

It was suggested that the CFD program developed could be used to predict buoyant airflow in solar chimneys. It was recommended that at least double-glazing should be used to prevent excessive condensation on the glazing and backdraughting in cold weather. The presence of heat pipes increased the pressure drop through the chimney and decreased thermal buoyancy. Thus implying that a solar chimney of considerable height would be needed in order to maintain acceptable ventilation flow rates. Taking advantage of negative wind pressure to aid the flow of air through the chimney would also help.

A similar CFD model was applied to the study of a Trombe wall (see Figure 1 7) for passive cooling of buildings (Gan [6]). The effect on the system by variation of temperature and heat gain; space between glazing and the storage wall; inlet width; wall height; and glazing type were investigated. In the paper, a comparison was carried out between the performance of a Trombe wall and a solar chimney. It was concluded that a solar chimney performs better for summer cooling because it possesses less flow resistance (at the chimney exit) and can thus achieve higher airflow rates.

Akbari and Borgers performed two numerical Trombe wall studies: one considering laminar convective flow [21], and the other considering turbulent convective flow [22] within the channel. Correlations for design purposes were presented based on their numerical results. For turbulent flow, the following correlation for flow rate as a function of total height, relative plate temperatures and the Grashof number (Gr) was given:

$$Q = 10^{-(C \cdot D \log L^\alpha)}$$

(2.16)

where

$$C = E\Delta T^\beta$$

$$\alpha = 0.260 + 1.940(\log Gr - 4)^{1.2}$$

$$\beta = -1.134(\log Gr)^{-1.768}$$

$$D = 10^{(1.931 - 0.544 \log Gr)}$$

$$E = -0.7628 + 0.3984 \log Gr$$

This study considered only dynamic head losses at the exit, where the loss coefficient was taken as $k = 1$. However, referring to Akbari and Borgers' [21] study, Tichy [23] stated that the actual loss coefficient (k) for combined inlet and exit losses is

33

probably $2 < k < 5$ based on data given by ASHRAE [24]. These pressure losses are significant: for $k = 5$, the flow rate can be reduced by 70% compared to $k = 1$.

2.4 Discussion of Literature Review

As reported above, natural ventilation flow rate in a solar chimney system is dependent on the following parameters: height of the chimney, the temperature difference between the inside and outside of the chimney, which is again dependent on solar heat gain, the cross-sectional area of the chimney as well as opening areas and other restrictions along the flow path.

Most of the experimental studies reviewed used full-scale models, while only two used small-scale models. Unfortunately, the scope of many of these experimental investigations was limited. Perhaps the most enlightening work related to solar chimney ventilation was completed by Bouchair [2]. Some important results of his include the observation of an optimum chimney width for maximum ventilation, apparently occurring at the boundary layer thickness at the top of the chimney, and the influence of the chimney inlet area on the optimum chimney thickness and overall airflow rate.

Considering the analytical works, it can be seen that most researchers predict the ventilation flow rate through a solar chimney using some form of Equation (2.1). The main difference amongst the works was the way in which the internal chimney temperature was specified and the values specified for loss coefficients. The exception to this type of prediction tool came from Bouchair [19] in which he used semi-empirical relations for turbulent natural convection from a flat plate to determine the boundary layer flow next to the chimney walls.

The computational works also contributed to the understanding of solar chimney airflow and pressure losses through the system.

2.5 Objective of the Present Study

From the literature review, it can be seen that a limited amount of experimental investigations for solar chimney ventilation have been carried out. There are a number of uncertainties concerned with optimum chimney width, ventilation inlet design, and solar chimney height. For example, Bouchair [2] investigated the optimum chimney width, however, his tests were performed for both walls at the same temperature. In reality, there is more likely to be a constant heat flux along the outer wall, from solar radiation, with 40% of this heat reaching the unheated, inner wall by radiation [11]. Good understanding of how these key factors affect the ventilation flow rate is essential if solar chimneys are to be designed and operated effectively.

It is evident that airflow in a solar chimney is very complex, and this puts into doubt the ability of simplified analytical models to accurately predict airflow rate through the chimney. For instance, Equation (2.1) predicts increasing ventilation flow rate with increasing chimney width, but existing experimental data show this to be incorrect.

Additionally, most of the analytical models reviewed assume a simple temperature distribution within the solar chimney, but it is evident that the temperature can vary significantly, across both the chimney width and the chimney height (see Sandberg and Moshfegh [12] for example). It is thus necessary to investigate the accuracy of simplified analytical models, in predicting solar chimney ventilation flow rate, in order to test their limitations when used for design purposes.

35

Therefore, it is the objective of the present work to study the behavior of a solar chimney natural ventilation system, and to better understand the influence of key parameters on the ventilation flow rate. The study will be done by experiment, with constant solar radiation incident on a single chimney wall. The following parameters will be investigated:

- Incident solar radiation;
- Solar chimney width;
- Solar chimney height;
- Ventilation inlet area.

The experimental investigation will be carried out using a small-scale model of a solar chimney attached to a single-zone building. Ventilation flow rate will be measured and flow through the model will be observed.

Experimental measurements will be compared to two simple analytical models: one based on a uniform temperature distribution in the chimney, and another based on a linear temperature distribution in the chimney.

CHAPTER 3

EXPERIMENTAL SET-UP AND APPARATUS

3.1 Overview of Experiment

The experiment was performed using a small-scale perspex model, which

consisted of a solar chimney attached to a single room. The model was submerged in a

large glass tank filled with a salt-water solution. Current passing through a copper wire

cathode, positioned along the height of the outer chimney wall, produced a plume of fine

bubbles, which simulated the buoyancy effect within the chimney due to solar radiation:

the density difference between the bubble plume and the ambient fluid simulated density

differences caused by temperature differences produced by solar radiation.

The fine-bubble technique was developed by Chen and his colleagues [25], and

was used because it is simple, economical and compact compared to other building

ventilation modeling methods; particularly gas and brine-water modeling systems.

In gas modeling systems, similarity requirements are often hard to obtain and the

heating elements themselves are often awkward and difficult to operate. Brine-water

modeling systems have the following disadvantages: a large reservoir of fresh water is

required to ensure negligible salt levels in the environment; additional facilities are

required for the continuous injection of salt solution; and visual observations must be

turned upside-down because of the higher density of the salt solution compared to the

fresh water.

The fine-bubble method requires a simple electric circuit consisting of a constant

voltage DC power supply, a copper wire cathode, a graphite anode and a tank full of salt-

water. The required tank size varies with the nature of the experiment and the size of the model. Therefore, the need for awkward heating elements, visualization inversions, large reservoirs etc. is eliminated, thus simplifying the experimental method considerably. Chen and his colleagues have successfully applied the fine-bubble modeling technique to building ventilation applications (see [25] and [26]).
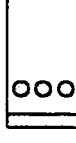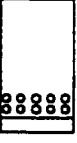
The velocity was measured at the room inlet and the solar chimney width varied for parameters of:

- Solar radiation incident on the solar chimney wall, at buoyancy fluxes of 122, 244, 367 and 489cm^4/s^3;

- Room inlet and chimney inlet geometry, considering four different opening configurations (modes) defined in Table 3.1;

- Solar chimney height, for 200 and 400mm;

- Solar chimney channel gap, from 5 to 30mm for the 200mm chimney and from 8 to 50mm for the 400mm chimney.

3.2 Experimental Set-up and Apparatus

The following components were used in the experiments: a perspex model, a large glass tank, a copper wire cathode, graphite anodes and a number of constant voltage DC power supplies. A video camera was used in the measurement of flow velocity. Figure 3.1 depicts the experimental set-up.

Table 3.1 Definition of modes (The schematic diagrams depict the wall into the room or chimney, with ventilation openings shaded).

Mode	Room Inlet			Chimney Inlet		
	Area (mm^2)	Opening Geometry	Schematic	Area (mm^2)	Opening Geometry	Schematic
I	1500	Rectangular		1500	Rectangular	
II	3000	Rectangular & circular		1500	Rectangular	
III	1500	Rectangular		3000	Rectangular & circular	
IV	3000	Rectangular & circular		3000	Rectangular & circular	

3.2.1 Glass Tank and Ambient Conditions

For the 200mm chimney height, the model was positioned in a large tank with dimensions of 0.9m (length) × 0.345m (depth) × 0.45m (height). A tank of the same length and depth was used for the 400mm high chimney, but with a tank height of 0.7m. Water was filtered before being poured into the tank to eliminate particles that could disturb the fluid flow or damage the cathode. Salt was then stirred into the fresh tank water, producing a salt-water solution, approx. 4.5 % (wt). Salt was added to increase

electrical conductivity A small amount of surfactant was added to the solution to reduce the effect of bubble coalescence.

Neutrally buoyant polystyrene particles were distributed in the tank to facilitate velocity measurement and flow visualization. The polystyrene particles were 0.8 – 1.0 μm in diameter, with a density of approximately 1030 kg/m³. Because the particles varied slightly in density, some would eventually settle to the bottom of the tank and some would float to the top. This required that the tank be stirred before the experiments to displace the settled and floating particles and distribute them evenly within the fluid. A period of time (approx. 20 minutes) was allowed after stirring so fluid velocities could settle before the experiments were performed, thus minimizing the stirring effect on experimental measurements.
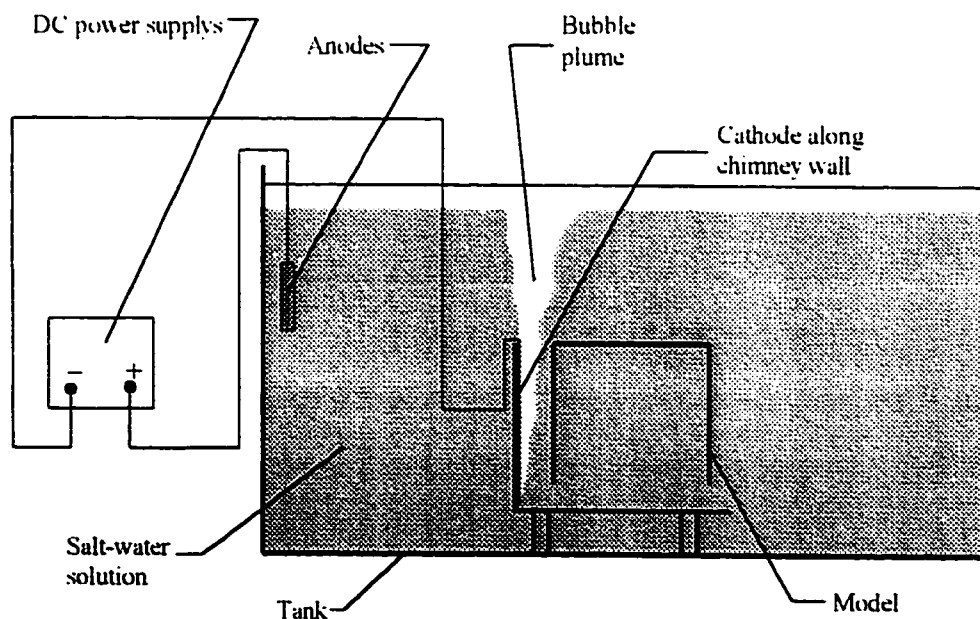
Figure 3.1 Schematic view of the experimental set-up.

3.2.2 Small-scale Solar Chimney Model

The small-scale model was comprised of a solar chimney attached to a 0.2m

(width) × 0.1m (depth) × 0.2m (height) room. See Figure 3.2 for details of the solar

chimney model and Figure 3.3 for photographs of the model. Figure 3.4 depicts the solar

chimney rig operating in the tank. The depth and height of the solar chimney were fixed

while its width was adjustable. A ruler attached to the side of the chimney was used to

measure the chimney width.

One 100mm × 15mm rectangular ventilation inlet and 3 × ϕ25mm circular

ventilation inlets were positioned in an exterior wall of the room, allowing ambient fluid

to travel into the room. There were one 100mm × 15mm rectangular and 10 × ϕ14mm

circular inlets in the wall between the room and the chimney, allowing fluid in the room

to travel into the chimney. The rectangular outlet area of the chimney varied with the

chimney width. Figure 3.2 shows the position and geometry of the openings.

Legs on the bottom of the model provided a space of 65mm between the floor of

the tank and the room. In order to investigate the effect of chimney height, a 200mm

extension to the chimney channel was attached to the original chimney, giving a total

height of 400mm.

3.2.3 Bubble Generating Equipment

Fine hydrogen bubbles, produced by a copper wire array cathode, provided

buoyancy forces in the chimney. The copper wire cathode consisted of numerous thin

wires (0.5mm in diameter) connected, by solder, at 90 degrees to two slightly thicker lead

wires (0.8mm in diameter for 200mm chimney height and 2.0mm in diameter for 400mm
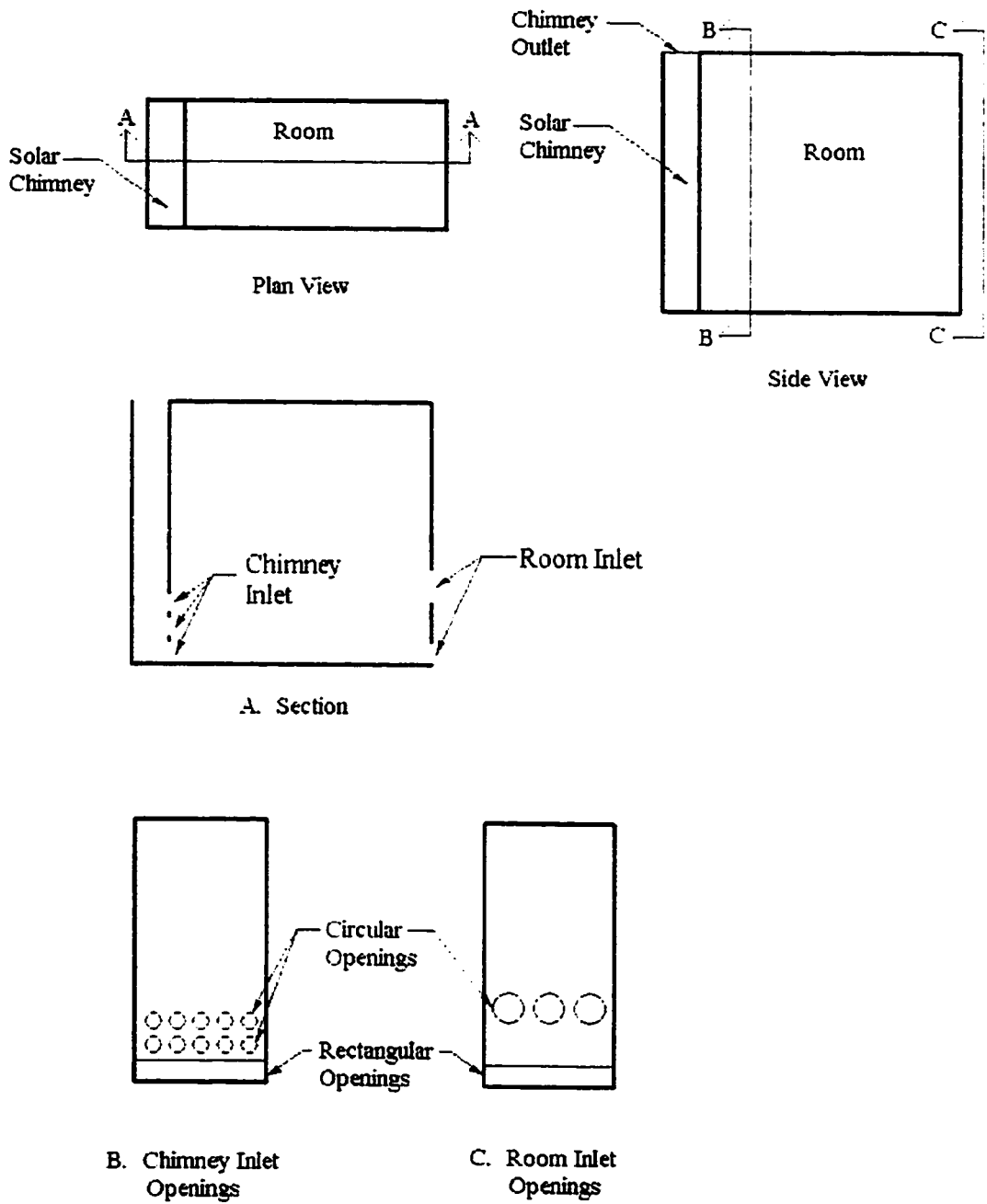
Figure 3.2 Details of the small-scale model with the 200mm high chimney.

42
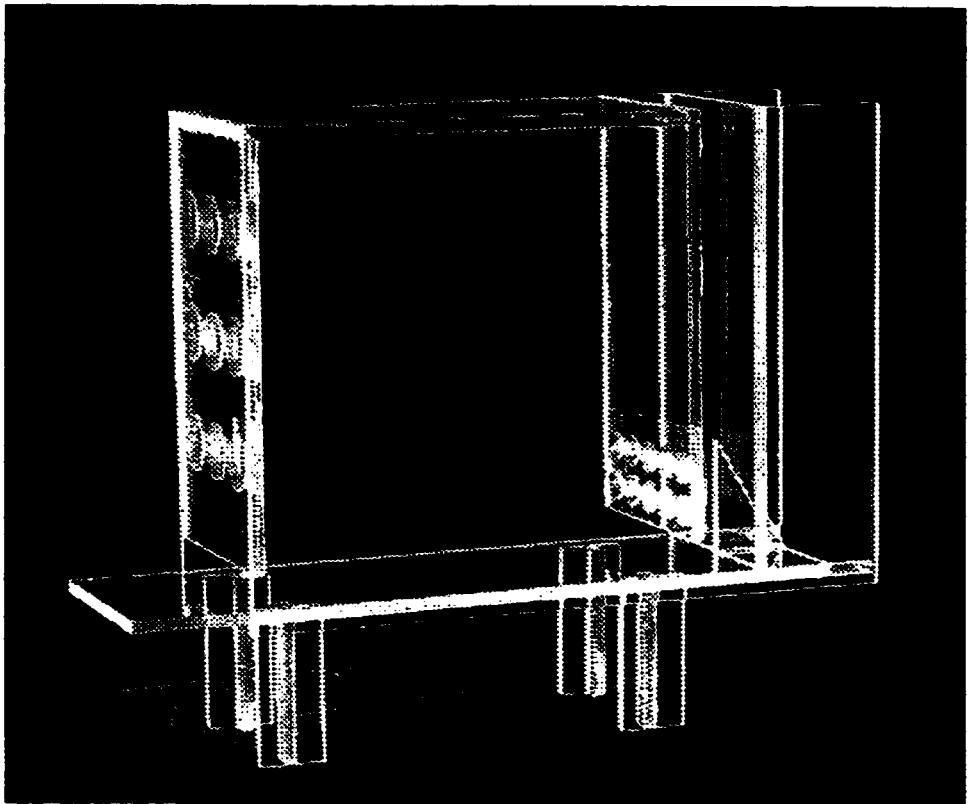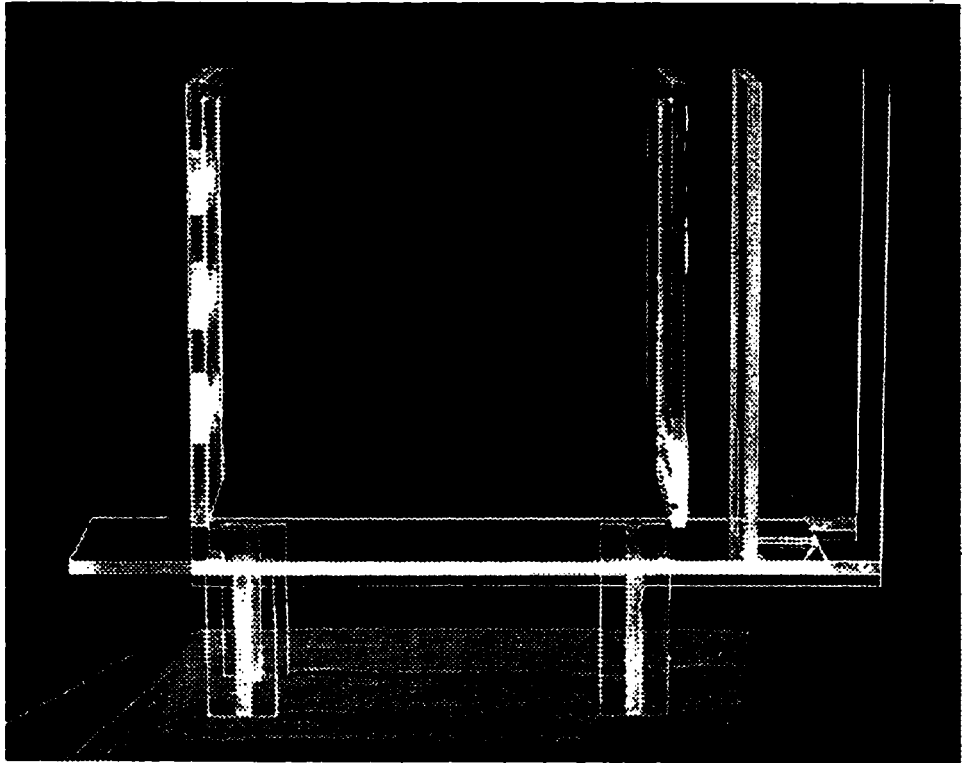
Figure 3.3 Photographs of the small-scale model.
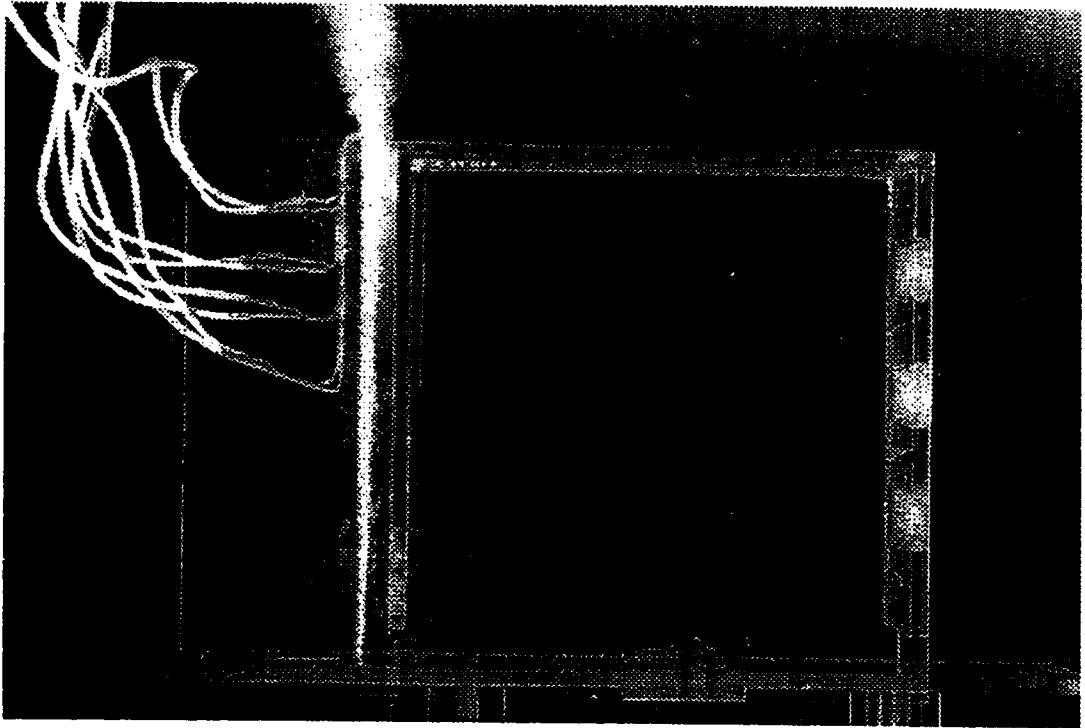
Figure 3.4 Solar chimney rig operating within the tank

chimney height). The cathode was attached to the outer chimney wall, as shown in Fig. 3.5. The smaller wires spanned the depth of the chimney (100mm), and were placed approximately 4 mm apart along the height of the chimney to provide an evenly distributed buoyancy flux from the wall. The thicker lead wires were coated in a two-part polyurethane gloss enamel. This waterproof coating prevented the thicker wires from producing bubbles too large for buoyancy simulation.

The copper wire cathode was split up into four parts for the 200mm chimney and two parts for the 400mm chimney. Division of the cathode was required because of the varying electrical resistance between the cathode and the anode, depending on the cathode position along the chimney height; e.g. resistance between the cathode and the

anode at mid-height of the chimney was larger than that at the top and bottom of the chimney. By splitting up the cathode, the voltage applied to the cathode could be varied for each section, depending on the resistance, to provide a more evenly distributed current along the wall. Dimensions of the cathode sections are shown in Figure 3.6 for both chimney heights.

The resistance along the height of the chimney was tested using a wire approximately 100mm in length (the depth of the chimney), and moving it from the bottom of the chimney to the top, taking measurements at small increments. These measurements were carried out at the smallest chimney widths encountered during the experiments where resistance variation was the greatest. The resistance distributions for the 200mm chimney with a 3mm width and the 400mm chimney with a 8mm width are shown in Figure 3.7.

When the electric circuit was closed, current traveled from a graphite anode, through the salt-water, and to the copper wire array cathode, from which hydrogen bubbles were generated. A typical graphite anode measured approximately 50-80mm (length) × 10mm (width) × 10mm (thickness). Anodes were constructed by first drilling a small hole in the top of a small piece of graphite. Then a cable was inserted into the hole, which was next filled with solder, and glued with Araldite epoxy resin to provide extra fix and waterproofing, see Figure 3.8.

.
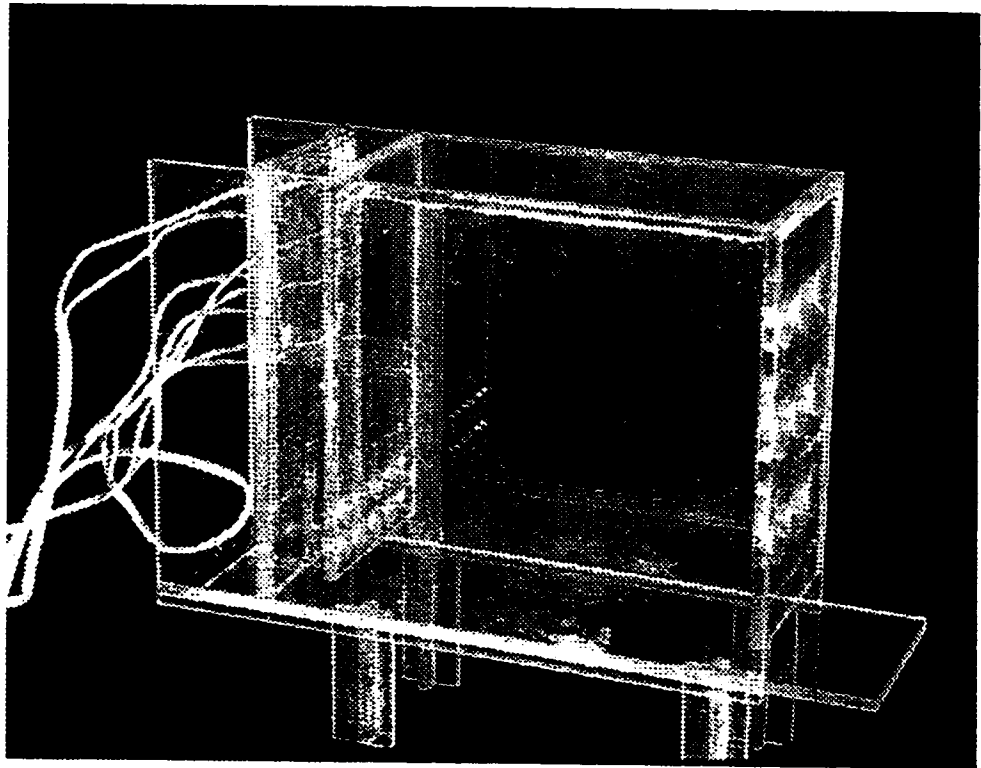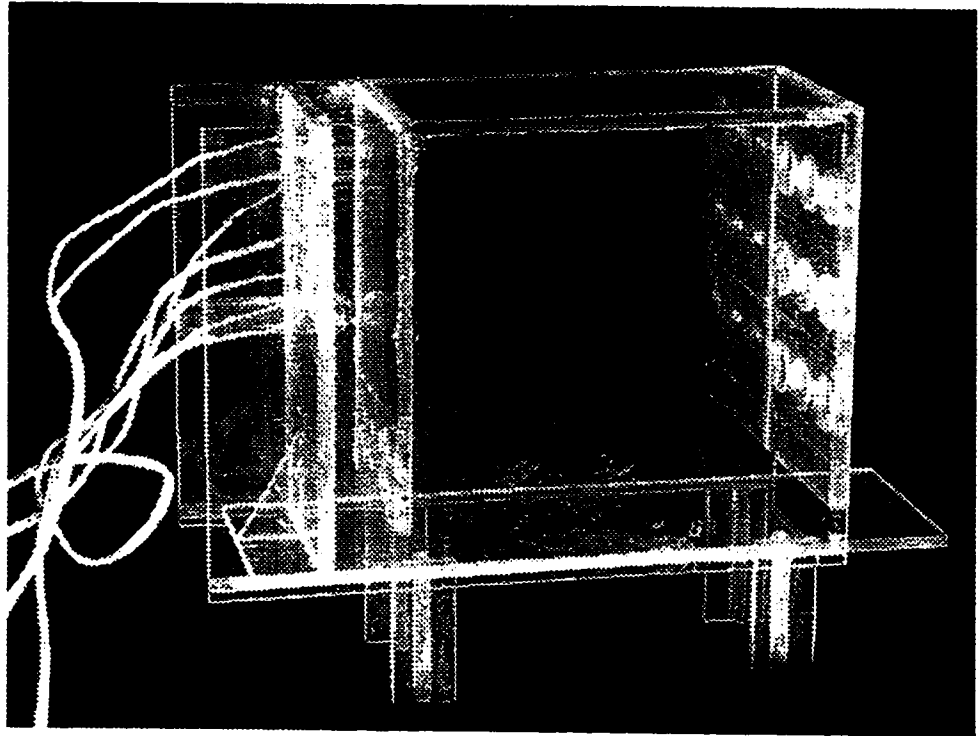
Figure 3.5 Photographs of the small-scale model with the copper wire cathode attached.
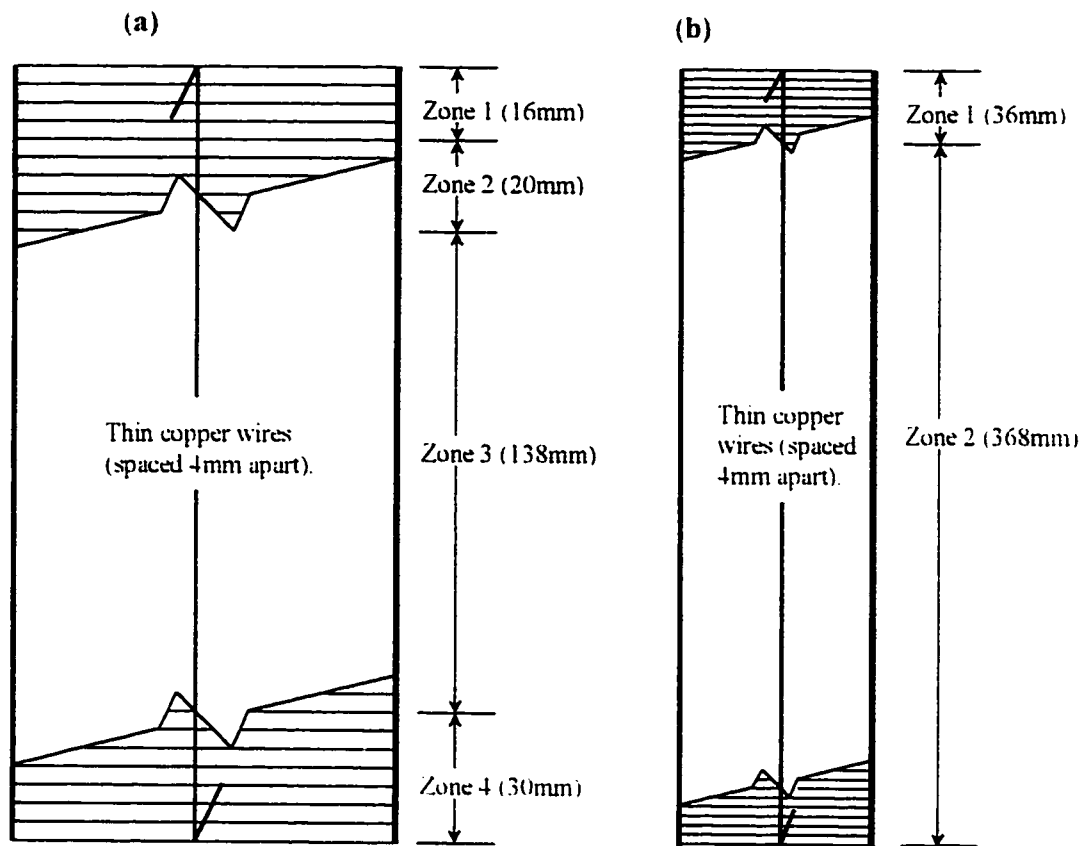
Figure 3.6 Zones and dimensions of cathode sections for **(a)** the 200mm high chimney

and **(b)** the 400mm high chimney.
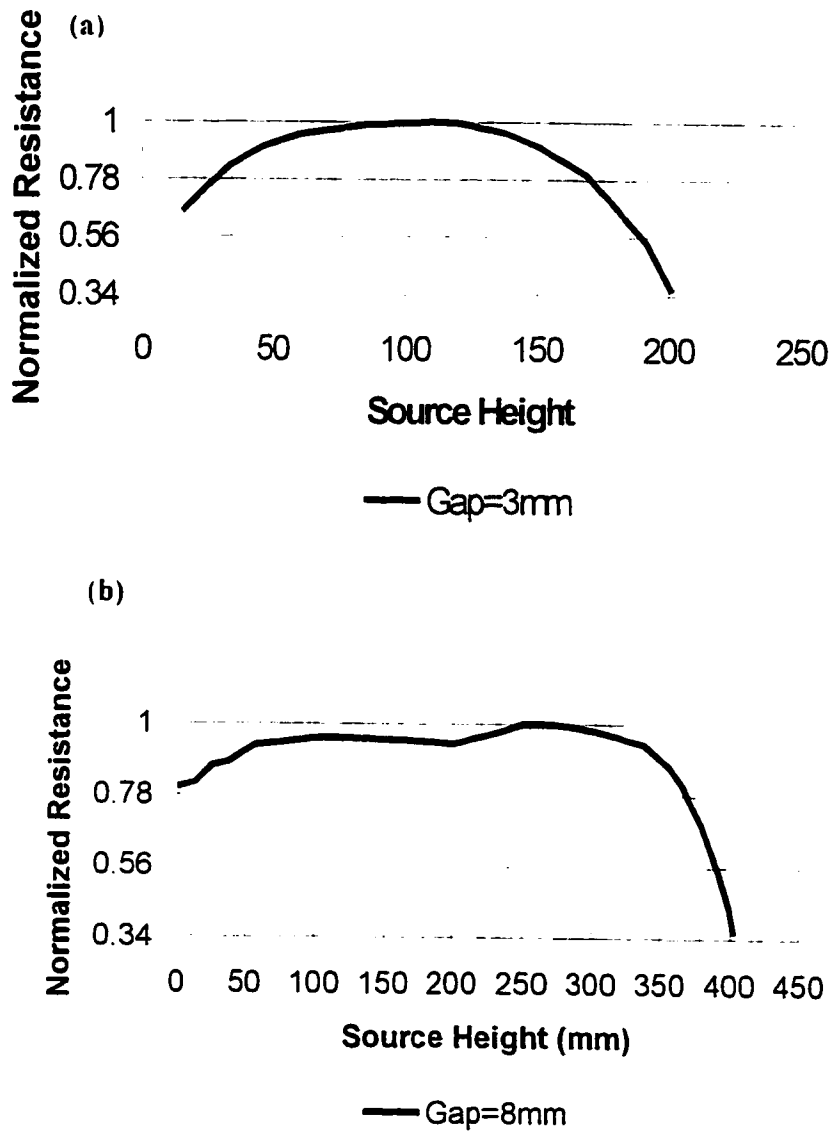
Figure 3.7 Distribution of resistance in the chimney for (a) the 200mm high chimney, and (b) the 400mm high chimney.

Since the cathode was split up into multiple sections, an anode and a constant voltage DC power supply were required for each section – four of each for the 200mm high chimney and two of each for the 400mm high chimney.
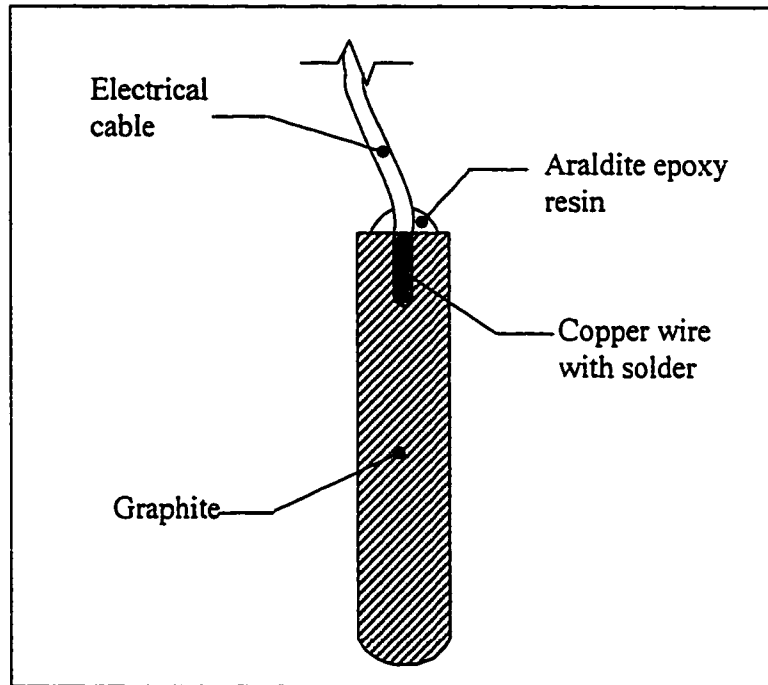
Figure 3.8 Section of a typical graphite anode.

The buoyancy flux (*B*), produced by the bubble plume, was calculated using the following relation:

$$B = gQ_g \frac{(\rho_s - \rho_g)}{\rho_s} \tag{3.1}$$

where Q_g is the gas flow rate from the cathode, which is determined by the current, and ρ_s and ρ_g are the densities of the salt-water and the hydrogen gas, respectively. Details for the calculation of buoyancy flux can be found in Appendix A. The effect of incident heat flux on the chimney was investigated by varying the buoyancy flux of the bubble plume

produced by the copper wire cathode. The buoyancy flux was varied simply by varying

the current through the cathode: i.e. by increasing the current, the hydrogen flow rate (Q_a)

was increased and. in turn, the buoyancy flux (B). The buoyancy flux is proportional to

the heat flow from the source (q), as follows [27]:

$$B = \frac{qg}{\rho C'_p T}$$

(3.2)

3.2.4 Velocity Measurement

In this work, there was difficulty in finding an effective and convenient method

for measuring the flow velocity due to the fact that the experiments were performed in

salt-water and low flow velocities were encountered. It was finally decided that the best

available method was a particle tracking technique, whereby neutrally buoyant particles

were timed, and hence the velocity determined, as they entered the room inlet.

Timing of the particles was accomplished by using a Panasonic S-VHS movie

camera (model NV-MS4) to record images of the particles entering the room inlet. The

images were played back frame-by-frame. and the number of video frames it took a

particle to travel a short distance of 7mm was counted. Knowing that the video played

back at 50 frames per second, the time could be determined simply by dividing the

counted number of frames by 50.

The average velocity, u_{ave}, was obtained from the average of 25 to 30

measurements:

$$u_{ave} = d/t$$

(3.3)

50

where t was the average time it took a particle to travel the 7mm distance (d) at the room inlet. The average ventilation flow rate (Q) through the building was then simply obtained from

$$Q = u_{ave} \times A_{ri} \qquad (3.4)$$

where A_{ri} is the area of the room ventilation inlet.

This method of velocity measurement was very tedious and time consuming. and proved to be the main disadvantage of the experimental method used.

3.3 Similarity

In the field of building ventilation, small-scale models offer a means of predicting the behavior of full-scale systems, or prototypes, without the extra cost. time and inconvenience often associated with testing a full-scale model. Scale factors are applied to measurements taken from the small-scale test to obtain full-scale quantities. However. this can be done only if the flows in the model and the prototype are dynamically and geometrically similar. Dynamic similarity requires that the dimensionless differential equations and boundary conditions describing both flows be identical. In other words, the ratio of forces acting on the model and the prototype must be constant and in the same direction. If both flows are to have the same dimensionless boundary conditions, then they must be geometrically similar, that is all solid surface boundaries of the model must be the same shape as the prototype and scaled by a constant factor.

Upon nondimensionalizing the governing differential equations and boundary conditions of the two flows, certain coefficients, or similarity parameters, will appear in the dimensionless form of the equations. Therefore, if the similarity condition is to be

satisfied (i.e. identical dimensionless governing equations describing both flows) the similarity parameters must have the same value for both the model and the prototype.

In buildings ventilated by means of natural convection, the appropriate similarity parameters are the Rayleigh (Ra) and the Prandtl (Pr) numbers, (or Schmidt number for natural convection driven by concentration differences) [27]. However, in turbulent dominated flows with sufficiently large Rayleigh numbers, buoyancy dominates and viscous effects become negligible; consequentially, the requirements for the Rayleigh and Prandtl numbers become unnecessary and the flow in the model and the prototype will be similar [27]. Turbulent flow dominates when $Ra \geq 10^{13}$ [27]. The Rayleigh number, for a plume generated by a heat source, is given by

$$Ra = \frac{g\beta q L^2}{k v D_T} \qquad (3.5)$$

where q is the constant heat flow from the heat source, β is the thermal expansion coefficient, L is the characteristic length of the system, k is the thermal conductivity, v is the kinetic viscosity and D_T is the thermal diffusivity. Since the buoyancy flux from a heat source in a building is given by Equation (3.2), Equation (3.5) can be rewritten as:

$$Ra = \frac{BL^2}{v D_T^2} \qquad (3.6)$$

Similarly, for natural ventilation in a model system driven by concentration differences, the Rayleigh number can be expressed as [25]:

$$Ra = \frac{BL^2}{v D_m^2} \qquad (3.7)$$

Where D_m is the diffusivity of the fluid from the buoyancy source to the ambient fluid.

To check that the similarity requirements are satisfied, let us make an example calculation using minimum values encountered in this work to estimate the Rayleigh number:

$B = 122 \text{cm}^4/\text{s}^3$

$L = 0.2 \text{ m}$

$\nu = 1 \times 10^{-6} \text{ m}^2/\text{s}$, the kinematic viscosity of water

$D_m = 5.10 \times 10^{-9} \text{ m}^2/\text{s}$ taken as the diffusivity of fine bubbles in water equal to that of hydrogen in water.

Inserting the above values into Equation (3.7) gives a Rayleigh number of $Ra = 1.88 \times 10^{15}$.

The free plume height can be calculated by rearranging Equation (3.7):

$$L = \sqrt{\frac{Ra D_m^2 \nu}{B}} \tag{3.8}$$

Considering the minimum values for B, ν and D_m given above and a Rayleigh number of $Ra = 10^{13}$, corresponding to the critical value for turbulent flow, Equation (3.8) gives the free plume height to be less than 15mm. Thus, all plume flows encountered in this experiment were fully turbulent.

When similarity between the model and its corresponding prototype is achieved, the following dimensionless relationships may be obtained [25]:

$$\left(\frac{B}{L^4 \theta^{-3}}\right)_{PT} = \left(\frac{B}{L^4 \theta^{-3}}\right)_{M} \tag{3.9}$$

where θ is the characteristic time scale, or

$$\left(\frac{B_{PT} L_M^4}{B_M L_{PT}^4}\right) = \left(\frac{\theta_M}{\theta_{PT}}\right)^3 \tag{3.10}$$

The term, θ_M / θ_{PT} in Equation (3.10) can be determined from known parameters of B_{PT}, B_M, L_{PT}, L_M. Therefore, the reduced gravity (g'), velocity (u) and the volumetric flow rate (Q) for the prototype may be obtained by the following expressions:

$$\frac{g'_{PT}}{g'_M} = \left(\frac{L_{PT}}{L_M}\right)\left(\frac{\theta_M}{\theta_{PT}}\right)^2 \tag{3.11}$$

$$\frac{u_{PT}}{u_M} = \left(\frac{L_{PT}}{L_M}\right)^3\left(\frac{\theta_M}{\theta_{PT}}\right) \tag{3.12}$$

and

$$\frac{Q_{PT}}{Q_M} = \left(\frac{L_{PT}}{L_M}\right)^3\left(\frac{\theta_M}{\theta_{PT}}\right) \tag{3.13}$$

For natural ventilation driven by temperature differences, we have

$$g' = g\left(\frac{\Delta\rho}{\rho}\right) = g\beta\Delta T \tag{3.14}$$

Similarly, for natural ventilation driven by concentration differences

$$g' = g\left(\frac{\Delta\rho}{\rho}\right) = g\beta_c\Delta\varphi \tag{3.15}$$

where φ is the concentration of the liquid and β_c is the volume expansion coefficient due to concentration changes.

Therefore, for a naturally ventilated building modelled by concentration driven systems, Equation (3.11) can be rewritten as

$$\frac{\beta\Delta T}{\beta_c\Delta\varphi} = \left(\frac{L_{PT}}{L_M}\right)\left(\frac{\theta_M}{\theta_{PT}}\right)^2 \tag{3.16}$$

For the fine bubble system, when φ is the gas volume fraction in the liquid, β_c is unity and Equation (3.11) becomes

$$\frac{\beta \Delta T}{\Delta \varphi} = \left(\frac{L_{PT}}{L_M}\right)\left(\frac{\theta_M}{\theta_{PT}}\right)^2 \qquad\qquad (3.17)$$

Equations (3.16) and (3.17) give the relationships of the concentration distributions on a model and the temperature distributions in its corresponding building prototype.

CHAPTER 4

EXPERIMENTAL RESULTS AND DISSCUSSION

4.1 Procedure

In this work, experiments were performed at chimney widths ranged from 5 to 30mm and 8 to 50mm for the 200mm and 400mm chimney, respectively. The effect of chimney width, buoyancy flux strength, chimney height and ventilation inlet area on the ventilation flow rate were investigated.

The effect of inlet area was tested for four different ventilation opening configurations, known as modes, at a buoyancy flux of $367cm^4/s^3$. The opening modes are categorized according to the combination of inlet areas to the room and chimney; see Table 3.1. The effect of source strength was investigated at buoyancy fluxes of 122, 244, 367 and $489cm^4/s^3$ while the inlet area was fixed at Mode (1). The effect of chimney height was investigated for heights of 200 and 400mm at opening Mode (1) and a buoyancy flux of $489cm^4/s^3$.

4.2 General Observations

4.2.1 Start-up of the Experiment

At the instant the DC power source was switched on, tiny bubbles began to form from the copper wire, rapidly producing a bubble plume along the chimney wall. Within a short period of time (approx. 5 to 10 seconds), the bubbles increased in number until they reached their maximum density for the given current, at which point the system

stabilized and velocity measurements could be taken. The sequence of photographs

shown in Figure 4.1 demonstrates this short, initial start-up period.

4.2.2 Observed Chimney Flow

The bubble plume entrained surrounding fluid, causing the fluid to flow up and

out of the chimney. Consequently, fluid exhausting from the top of the chimney induced

fluid into the room, via the room inlet, and then into the chimney, via the bottom chimney

inlet. Thus, the expected natural ventilation behavior of a solar chimney system was

reproduced.

As the particles entered the chimney, they were entrained into the bubble plume

and traveled up and out of the chimney. When the chimney width was increased. it was

observed that some particles were drawn into the chimney through the chimney outlet at

the top. They then traveled down the chimney until they were eventually entrained into

the bubble plume and traveled up and out of the chimney again. The observed backflow

caused a reduction in the overall flow rate through the system and will be further

examined below.

4.2.3 Observed Room Flow and Circulation

It was observed from particle traces that the flow, once drawn into the room inlet,

traveled in a fairly straight line towards the chimney inlet. However, not all particles

traveled straight into the chimney: some began traveling in the stream from the room inlet

towards the chimney, but then as they approached the chimney inlet, they traveled up,

away from the inlet and circulated around the room before being entrained into the jet
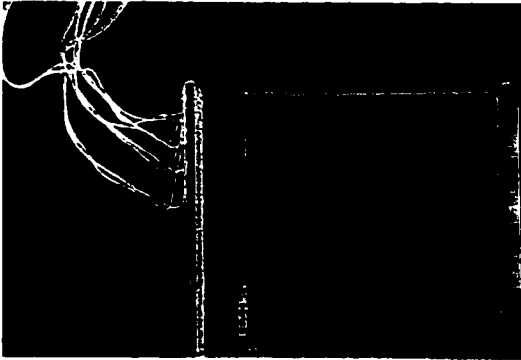
(1) (2)
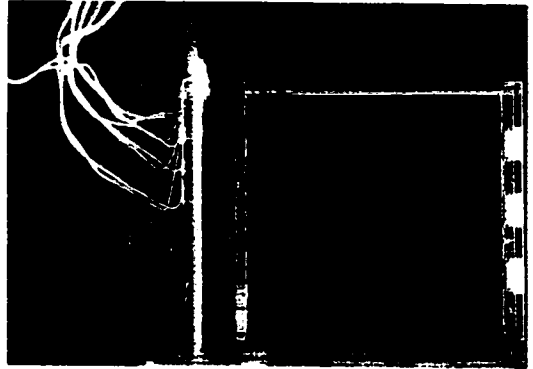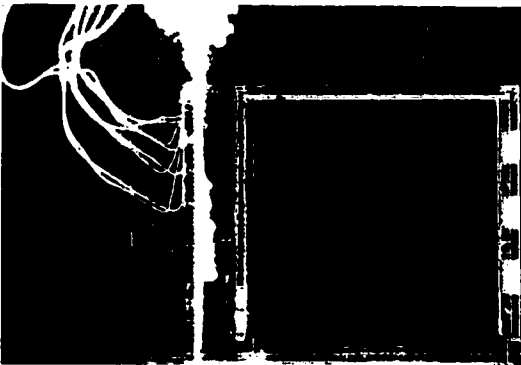
(3) (4)

(5)
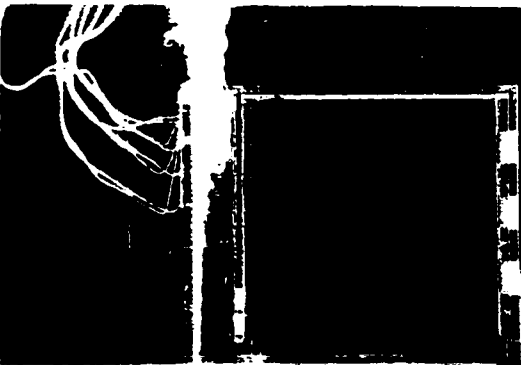
Figure 4.1 Start-up of the bubble plume.

again (see Figure 4.2). The observed circulation was due to the viscosity of fluid, causing

surrounding fluid to follow the stream as it traveled towards the chimney inlet. However,

the inlet area could not accommodate this extra flow, and as a result fluid "peeled" off the

stream and caused circulation in the room. In addition, the circulation appeared to

increase as the velocity of entering fluid increased.
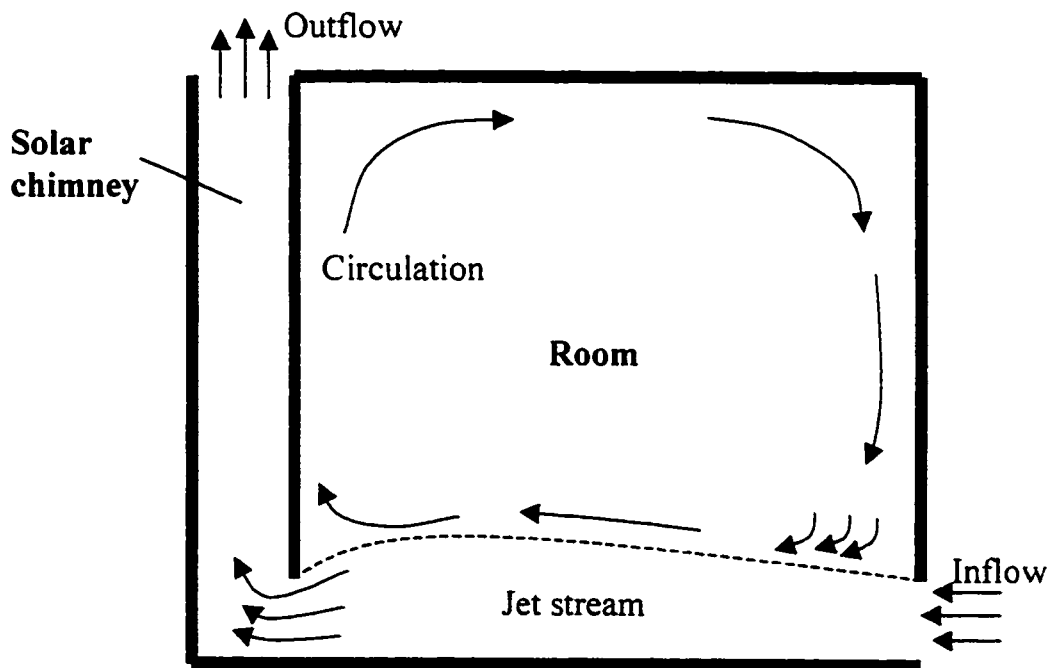
Figure 4.2 Schematic of the observed circulation within the room.

Several studies reported lack of circulation in solar chimney ventilated buildings.

For example, Bouchair [2] reported that observations made with smoke traces indicated

that fluid flowed in a streamline from the room inlet to the chimney inlet. In this case,

failure to note circulation in the room was probably due to airflow velocities being too

low to cause entrainment and therefore circulation. The present study suggests that if the solar chimney is well designed, air may be induced into the building at velocities high enough to cause circulation in the room, thus remedying, to a degree, the problem of "short-circuiting". It should be noted, however, that air movement within a typical building can be very complex, given possible obstructions, heat sources, and other aspects affecting fluid flow. As a result, many factors must be taken into account to ensure that adequate fresh air reaches the occupants.

Researchers such as Bouchair [2] and Barozzi [3] used solar chimneys for cross-ventilation purposes, and recommended that windows (or whatever ventilation inlet device used) be placed such that incoming fresh air could affect most of the occupants within the building. Other ventilation strategies may also be put in place, such as displacement ventilation, in which a layer of polluted air is stratified at the top of the room, thereby leaving fresh air in the bottom, breathing zone. In this case, the chimney inlet would have to be placed at the top of the room.

4.3 Results and Discussion

4.3.1 Effect of Source Strength

Figure 4.3 shows the effect of source strength on the ventilation flow rate, in terms of air change rate per hour. The air change rate per hour is defined by

$$ACH = \frac{Q}{V} \times 3600 \tag{4.1}$$

where V is the volume of the room (m³) and the ventilation flow rate, Q, is in the units m³/s.

It can be seen that increasing the buoyancy flux in the chimney caused a general increase in flow rate through the system. This is to be expected, because increasing the heat flux into the chimney increases the temperature of fluid within the chimney and, hence, the temperature difference between the chimney and outside fluid. This, in turn, increases the driving pressure and the ventilation flow rate.
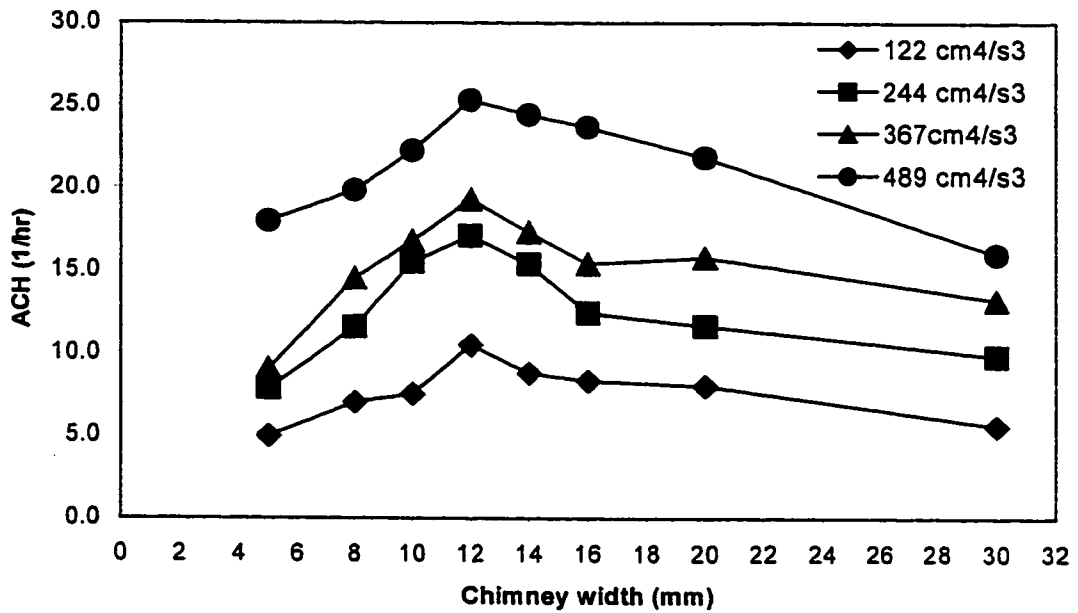
Figure 4.3 The effect of cavity width and source strength on ventilation rate.

Further observation of this figure reveals that, as the chimney width was increased from its starting position of 5mm, the air change rate in the room increased until the chimney width reached about 12mm. As the chimney width was increased beyond this point, the air change rate decreased. The maximum flow rate occurring at a chimney width of 12 mm signifies an optimum.

It can also be observed from Figure 4.3 that the optimum chimney width is independent of the buoyancy flux strength. Bouchair [2] implied similar results, where the optimum chimney width was independent of the temperature difference along the wall. More information on the effect of solar chimney width is detailed in the section below.

The independence of source strength and the optimal solar chimney width has obvious design advantages: the solar chimney may be designed according to its optimum width and the chimney will ventilate at its maximum rate for the given solar radiation intensity. This is important because the intensity of the sun can vary significantly, not only throughout the day, but also throughout the duration of the year. However, there are other factors to consider in the solar chimney design that affect the optimum chimney width, i.e. inlet areas and pressure losses, which will be discussed further below.

4.3.2 Effect of Chimney Width

It may be seen in Figure 4.3 that there is an optimum chimney width, occurring at around 12mm, at which the chimney provides maximum ventilation under, otherwise, the same conditions.

During the experiments, it was observed that as the chimney width was increased beyond a certain point (which was later found to be the optimum chimney width) fluid was sucked back into the chimney outlet near the "unheated" wall. Eventually the down-flowing particles would get entrained in the up-flowing fluid within the bubble plume and rise up, out of the chimney. The polystyrene particles within the tank allowed visualization of this. It was also observed that as the chimney width was increased wider

62

and wider, particles penetrated greater distances down the chimney. Figures 4.4 to 4.6 show the chimney at widths less than, equal to and greater than the optimum and Figure 4.7 shows a schematic view of the observed backflow in the chimney. With a further increase in the chimney width there was an increase in flow reversal and consequentially a reduction in net flow through the system.

As was discussed in the literature review, similar results and observations were found by Bouchair [2], in which a 2m solar chimney was used. Smoke visualization revealed that as the chimney was increased beyond its optimum width, backflow occurred in the middle of the chimney. Bouchair [2] suggested that this backflow was caused by separation of the boundary layers. Therefore, Bouchair suggested that the optimum chimney width occurred at the boundary layer thickness at the top of the chimney. He confirmed this with calculations using Equation (2.10).

Backflow in the chimney can be explained as follows: as the chimney width was extended beyond the boundary layer thickness, up-flowing fluid within the buoyancy plume created a region of low pressure near the unheated wall. This allowed ambient fluid to flow down the chimney near the unheated wall and supply the up-flowing stream of fluid to conserve mass. Since the up-flowing fluid was now partly supplied with recirculated fluid, less fluid was required from the chimney inlet at the bottom, therefore reducing the ventilation flow rate through the room. As the chimney was set wider and wider, more backflow occurred with a consequent decrease in ventilation flow rate.

Bouchair [2] found that the optimum chimney width was about one-tenth of the chimney height. In the present experiment, the optimum chimney width is found to be about one-seventeenth of the height for Modes (I) and (II), and one-twelfth of the height

Figure 4.4 The solar chimney at a width less than the optimum.

Figure 4.5 The solar chimney at the optimum width.
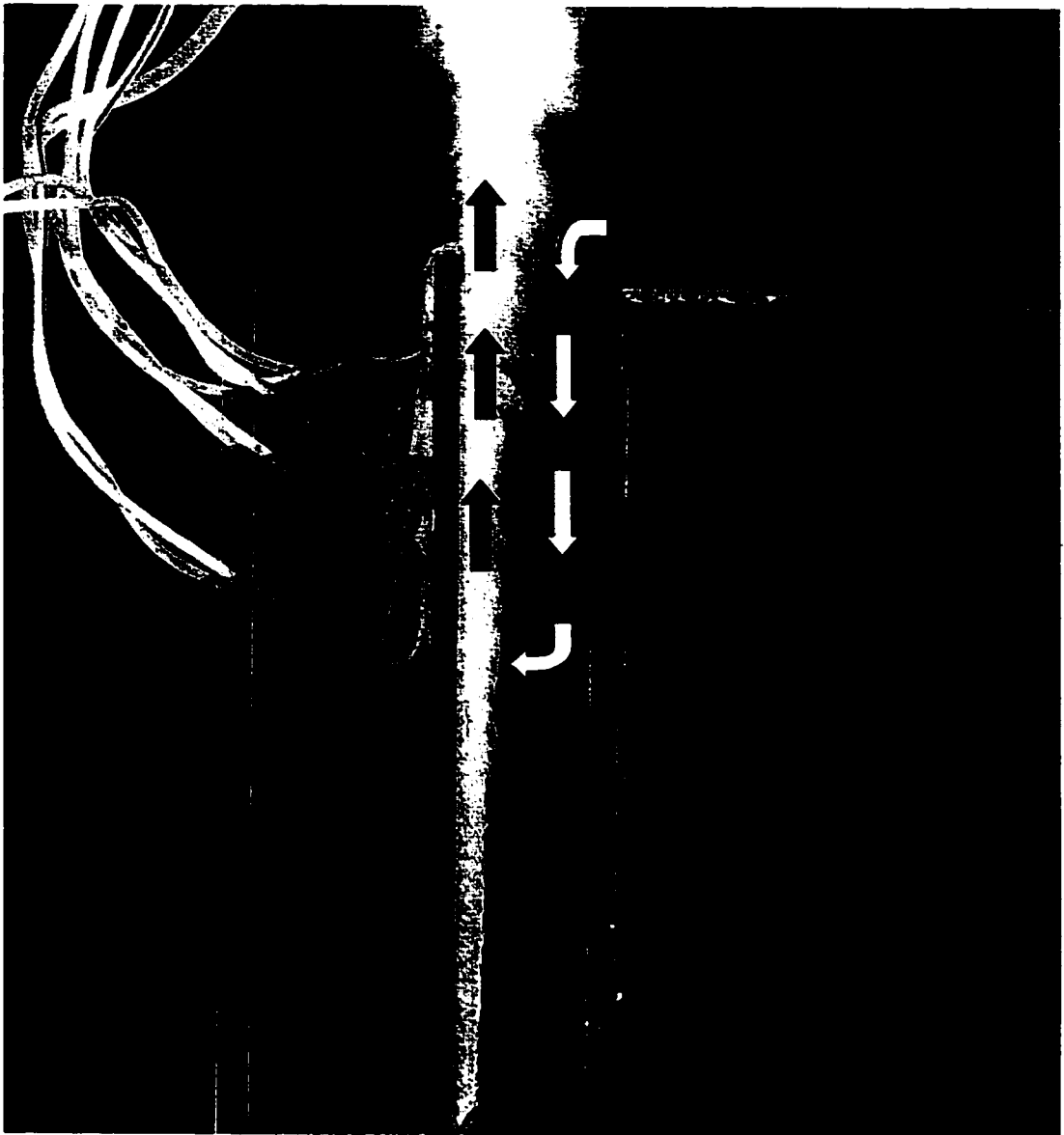
Figure 4.6 The solar chimney at a width greater than the optimum (the arrows represent the observed backflow in the chimney).

for Modes (III) and (IV). Thus the optimum chimney width in this work was found to be less than that found by Bouchair [2].
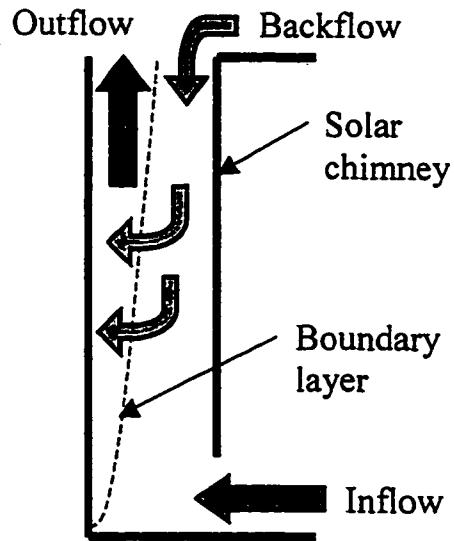
Figure 4.7 Schematic view of the backflow in the solar chimney.

The main reason for the discrepancy between Bouchair's results and the present work (for a given inlet area) is due to the fact that Bouchair had two walls of the solar chimney heated, while the present experiment had only one wall "heated". When both sides of the chimney cavity are heated, two boundary layers are created, enabled a wider chimney width to be achieved before backflow occurs, compared to that when a single boundary layer exists from a singularly heated wall. Since the optimum chimney width occurred at the boundary layer thickness, Bouchair achieved greater optimum chimney widths than those occurring in the present study.

Another factor to consider when comparing results with Bouchair is the difference in the type of heating condition applied to the chimney wall. That is, Bouchair specified a constant temperature condition, while a constant heat flux condition was specified in the

present study. Although this factor is not as important compared to the two versus one heated walls, imposing a constant wall temperature is likely to affect the boundary layer thickness differently than imposing constant heat flux.

It was found that the optimum chimney width was dependent on the chimney inlet area, where larger inlet areas (Mode (III) and (IV)) resulted in a larger optimal chimney width than at the smaller inlet areas (Modes (I) and (II)). The effect of inlet geometry is examined further in the next section.

4.3.3 Effect of Inlet Geometry

Variation of the room and chimney inlet areas had a significant affect on both the ventilation flow rate and the optimum chimney width. Figure 5.8 shows the experimental ventilation rate obtained for the four opening modes, at a buoyancy flux of $367 cm^4/s^3$. From this figure it can be seen that, in general, the larger the inlet area the larger the flow rate. This is to be expected: a larger inlet area allows greater flow through the system, as suggested by Equation (2.1).

From Figure 4.8, it is seen that much higher flow rates could be achieved with opening Modes (III) and (IV), compared to Modes (I) and (II). This suggests that increasing the chimney inlet area is more effective than increasing the room inlet area. The reason is that, greater pressure losses exist at the chimney inlet due to the 90°- elbow entrance from room into the chimney shaft, compared to the straight-through room inlet. Consequently, increasing the chimney inlet area is more effective in relieving pressure losses through the system than increasing the room inlet.

67
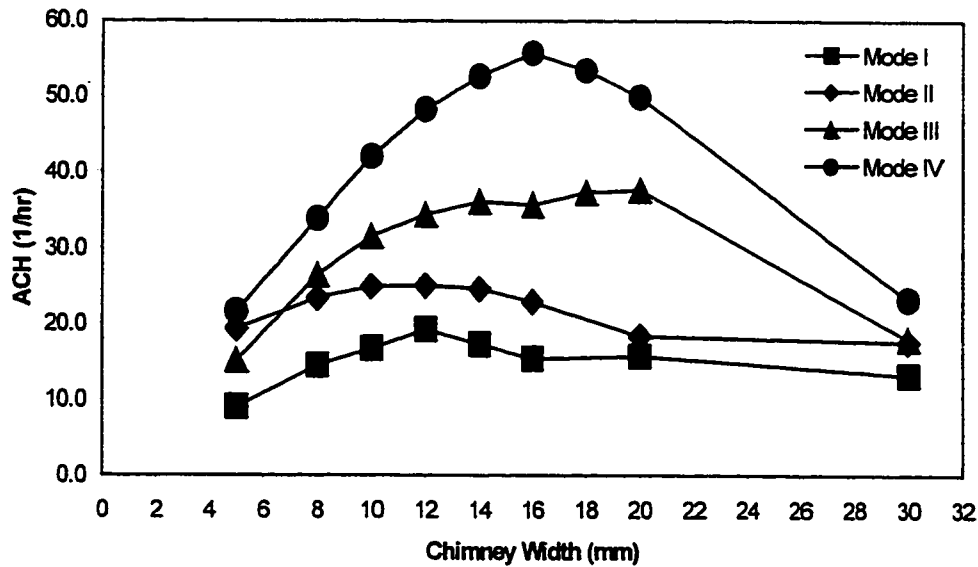
Figure 4.8 The effect of ventilation inlet geometry on the ventilation rate.

The decrease in pressure losses by increasing the chimney inlet area becomes

more apparent for medium to large chimney widths – for narrow chimney widths, friction

losses in the chimney are more critical. Bouchair [2] and Gan [6] noted similar results, in

which case both authors were able to increase airflow rates by increasing the inlet area at

medium to large chimney widths.

Further inspection of Figure 4.8 reveals a shift in the optimum chimney width, it

becoming significantly larger for Modes (III) and (IV) at around 16 – 18mm. At mode

(II), the optimum is about the same as it is at Mode (I), occurring between 10 and 14 mm.

Again, Bouchair [19] reported similar results, where he showed that increasing the

chimney inlet increased the optimum chimney width.

It is not quite clear why reducing the pressure losses into the chimney increased

the optimum chimney width. Indeed, Equation (2.9) appears to offer little insight into this

phenomenon since, under normal solar chimney operating conditions, it can be shown that the boundary layer thickness depends on the height of the chimney and on the difference in temperature between the chimney and the ambient:

$$b \propto \Delta T^{-0.1} h^{0.7} \tag{4.2}$$

Given that the variation of temperature difference, ΔT, is usually small under normal solar chimney operating conditions and that it is raised to a small power, its dependence of the boundary layer thickness (b) becomes insignificant, i.e.

$$b \propto h^{0.7} \tag{4.3}$$

Indeed, Bouchair [19] considered this when he simplified Equation (2.9) to obtain Equation (2.10). Therefore, according to relation (4.3), the boundary layer thickness is solely dependant on the height of the chimney (thus confirming the above results, which showed that the optimum chimney width was independent of source strength). But results shown in Figure 4.8 and results reported by Bouchair himself show that the optimum chimney width, which supposedly occurs at the boundary layer thickness at the top of the chimney, also depends on the opening area of the inlet. The reason that Equation (2.9) does not show the influence of pressure loss on the boundary layer thickness is because it was developed for a vertical flat plate, and therefore the effect of inlet pressure losses are not considered. This suggests that Equation (2.9) has limitations in its prediction of boundary layer thickness in a vertical channel, and this is compounded by the fact that Equation (2.10) could not predict the Bouchair's [19] optimum chimney width at an inlet height of 0.4m (as mentioned in Section 2.2).

When the experiment was performed at Modes (III) and (IV), where there was a large inlet to the chimney, increased mixing of the bubble plume in the chimney channel

was observed. A substantial increase in the flow velocity, caused by decreased flow resistance with the large inlet area, allowed fluid entering the chimney inlet to impinge on the chimney wall and disperse the bubble plume. Figure 4.9 displays a photograph of the chimney cavity with a large chimney inlet, in which it is seen that the bubble plume is widely dispersed within the channel. Figure 4.10 is a schematic view of the observed flow as it entered the chimney inlet. Observations suggested that the entering fluid was, at
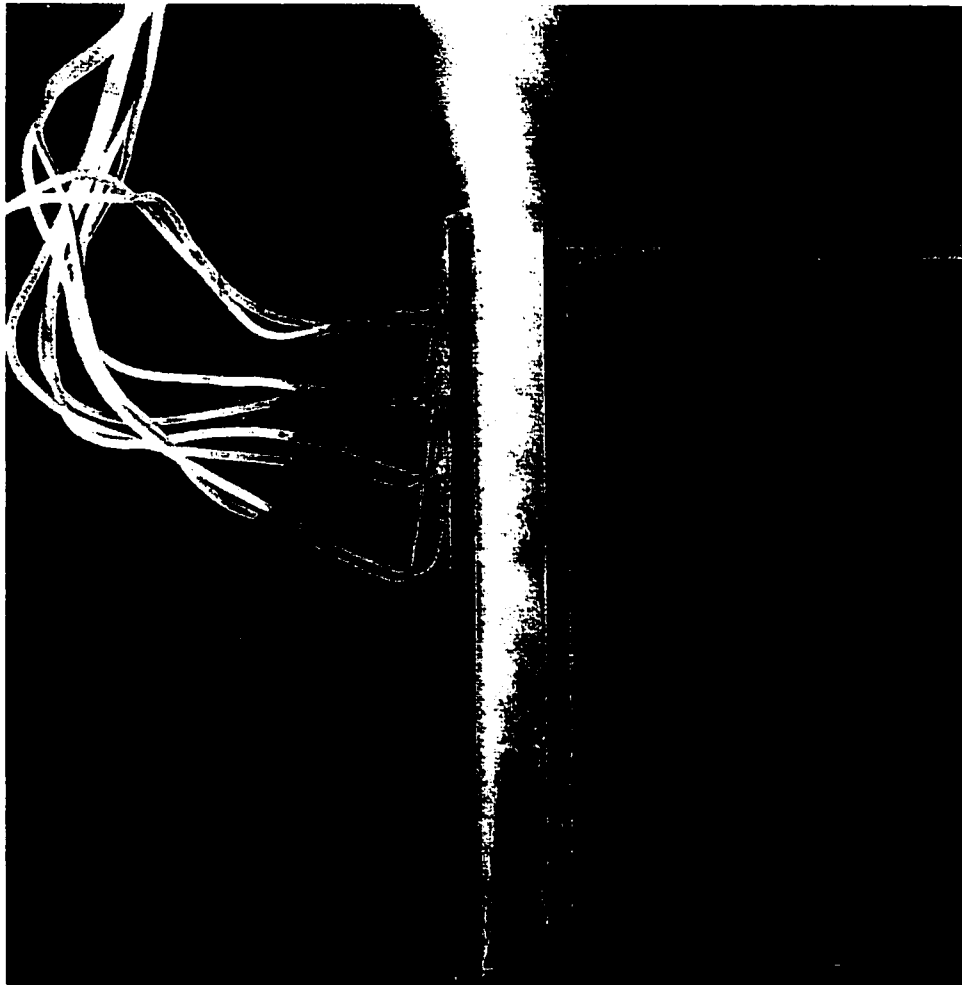
Figure 4.9 Mixing of the bubble plume with a large chimney ventilation inlet.
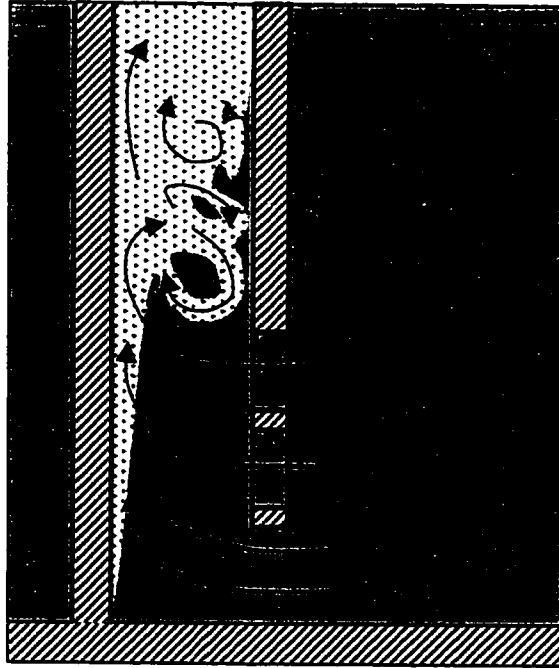
Figure 4.10 Schematic diagram of the observed plume mixing.

least locally, destroying the boundary layer. Consequently, the temperature distribution

within the chimney became more uniform than it was for the smaller chimney inlet

openings of Modes (I) and (II). Figure 4.11 illustrates the possible temperature

distributions for the small and large chimney inlets. With a more uniform temperature

distribution, greater flow rates could be achieved because the average temperature across

the chimney was higher, consequently producing higher stack pressure.

4.3.4 Effect of Solar Chimney Height

To evaluate the effect of the chimney channel height, tests were performed for heights of

200mm and 400mm. The tests were carried out at a buoyancy flux of 489 cm^4/s^3 and at

opening Mode (I). The results are shown in Figure 4.12, along with the results obtained

for the 200mm chimney at the same source strength and opening mode.
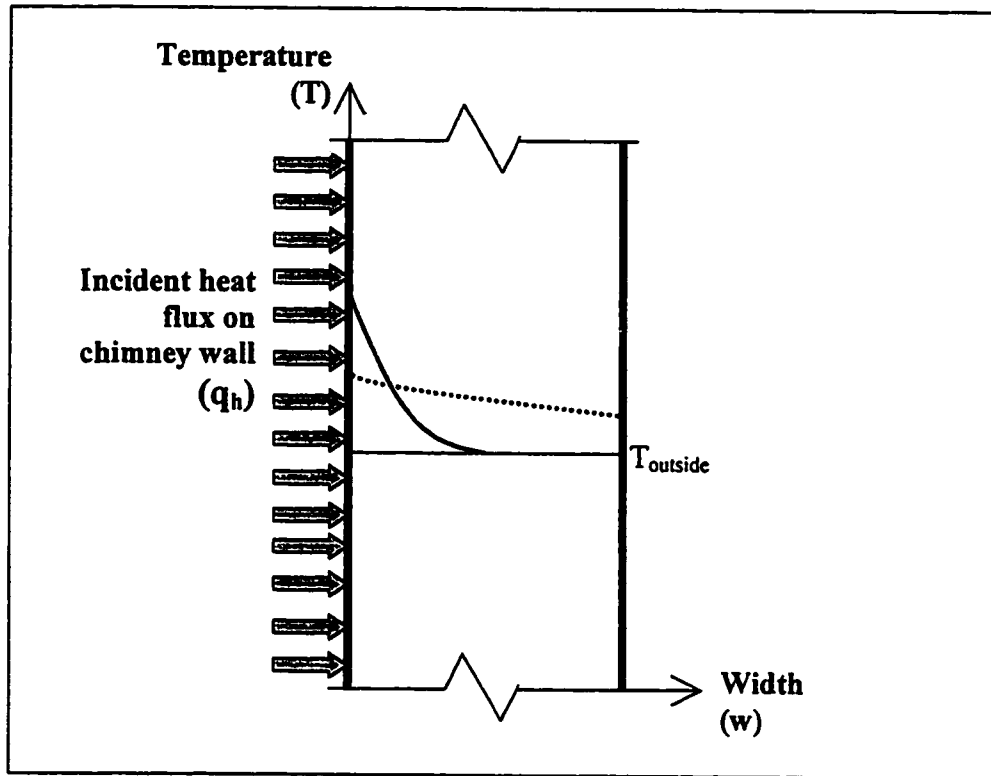
Figure 4.11 The possible temperature distribution in the solar chimney for a small inlet

(shown with solid line) and a large chimney inlet (shown with dotted line).

It can be seen that the optimum chimney width occurs at around 24mm for the

400mm chimney; twice the width encountered for the 200mm chimney. Such results

imply a linear relationship between the chimney height and the optimum chimney width

(refer to Figure 4.13). In other words, the optimum aspect ratio (chimney height:

optimum chimney width) remained fixed. If indeed the optimum chimney width is an

indication of the boundary layer thickness, then it appears that the boundary layer varies

linearly along the height of the uniformly heated chimney wall.
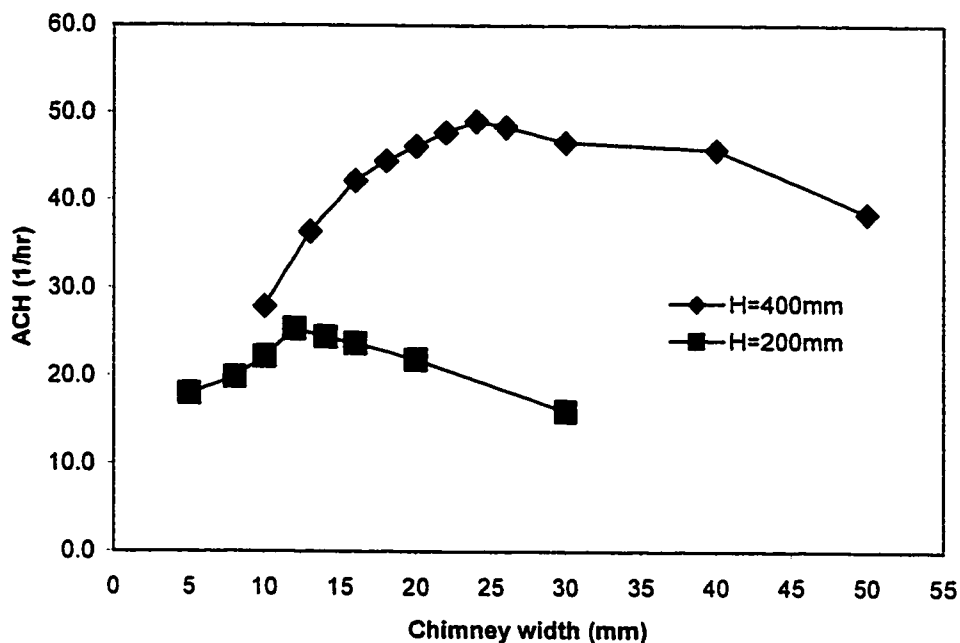
Figure 4.12 The effect of chimney height on the ventilation rate.

Swainson's [14] experiment indicated different results: the height varied non-

linearly with optimum width; instead, it closely following the relation given by Equation

(2.9). Thus the optimum aspect ratio did not remain fixed, but increased with chimney

height

The reason for the discrepancy may be due to the limited amount of points

measured in the present experiment, resulting in the inability to see the fairly subtle non-

linear relationship that Swainson found. Another reason for the difference may be due to

the fact that Equation (2.9) was derived for a wall at constant temperature and may not

apply to the constant heat flux condition.
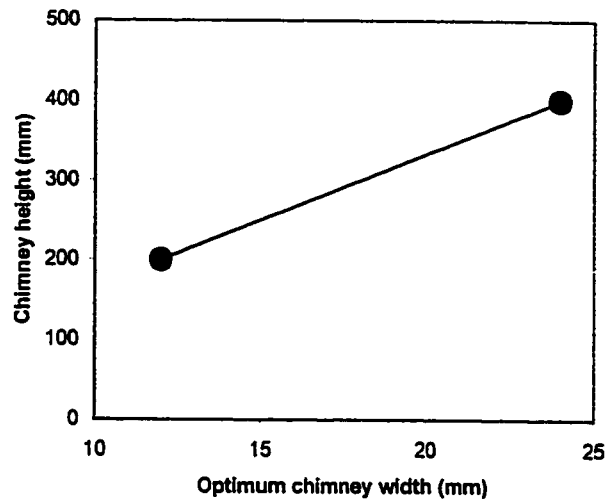
Figure 4.13 Relationship between the solar chimney height and
the optimum chimney width.

Referring again to Figure 4.12, it is noted that the air change rate measured at the optimum chimney width for the 400mm chimney is almost twice that measured for the 200mm chimney. Therefore, it appears that doubling the chimney height doubles the obtainable ventilation flow rate. These results suggest that increasing the chimney height is an effective way of increasing flow rate.

Interestingly, it was observed that mixing of the bubble plume occurred at the higher chimney, similar to that observed for a large chimney inlet. Again, the mixing was caused by high velocity fluid entering the chimney inlet and dispersing the bubble plume. However, in this case, high fluid velocity was caused by the increased chimney height, not from the decrease in pressure losses associated with the large chimney inlet area. Indeed, the height experiments were performed at mode (I), where the chimney inlet is small.

4.4 Uncertainty analysis

4.4.1 Copper Wire Deterioration

It was observed during the experiments that bottom wires on the top two sections of the cathode deteriorated with time, this was particularly apparent for experiments done for the 200mm chimney. The rate of deterioration depended on the current passing through the system, with higher currents causing faster deterioration. The higher voltage in the large section (Zone 3) caused current from there to flow to the smaller sections (Zones 1 and 2), causing deterioration (see Figure. 3.6 for location of cathode sections). It was clear that the deterioration of copper wire would affect the hydrogen gas bubble production rate. However, the influence was calculated to be within 2.7% (refer to Appendix B).

4.4.2 Repeatability of Velocity Measurements

Several trials were carried out to test the repeatability of the experimental technique; the results are shown Appendix C. Retrials were performed at Modes (I), (II) and (III) at a buoyancy flux $367cm^4/s^3$. It was found that the retrials were within ± 5%, ± 2.1%, and ± 2.9% for Modes (I), (II) and (III), respectively. Therefore, the repeatability of the experiments was quite satisfactory.

CHAPTER 5

ANALYTICAL MODELS

It is useful for designers to have simple, general tools for the prediction of ventilation performance of natural ventilation systems such as a solar chimney. Applying experimental modeling or CFD simulations to each new design situation can be expensive and time consuming. Therefore, it is important that a prediction tool for solar chimney ventilation exists to ensure its widespread use and effective performance. The most common and simple prediction tool found in literature is that used for stack effect ventilation, given by Equation (2.1).

In this work, similar theoretical models were considered, except the ventilation flow rate was put in terms of buoyancy flux, allowing convenient comparison with the experimental results. Two models were developed based on different temperature conditions within the solar chimney: (1) a model that assumes a uniform temperature distribution throughout the solar chimney, i.e. the fluid in the chimney is fully mixed; and (2) a model that assumes a linear temperature distribution in the solar chimney (see Fig. 5.1). Both models were developed considering only stack pressure.

5.1 Uniform Temperature in the Solar Chimney – Model 1

A uniform temperature distribution assumption is a common simplifying assumption used in airflow modeling for the purpose of determining the pressure drop across a given zone. For Model 1, the building is divided into two zones – the room and the solar chimney – and each zone is assumed to have a uniform temperature. Since there

76

are no heat sources in the room, the temperature in the room is the same as the ambient

Therefore the driving pressure, the stack pressure, comes only from the solar chimney.

At steady state conditions, the stack pressure must be equal to the pressure losses

through the system, thus we have:

$$\Delta P_s = \Delta P_L \tag{5.1}$$

where ΔP_s is the stack pressure and ΔP_L is the total pressure loss through the system. The

stack pressure, ΔP_s, is given by

$$\Delta P_s = \int_0^H (\rho_a - \rho_i) g \, dh \tag{5.2}$$

where the fluid density within the chimney, ρ_i, is constant since the temperature within

the chimney is assumed constant. Therefore, integration yields
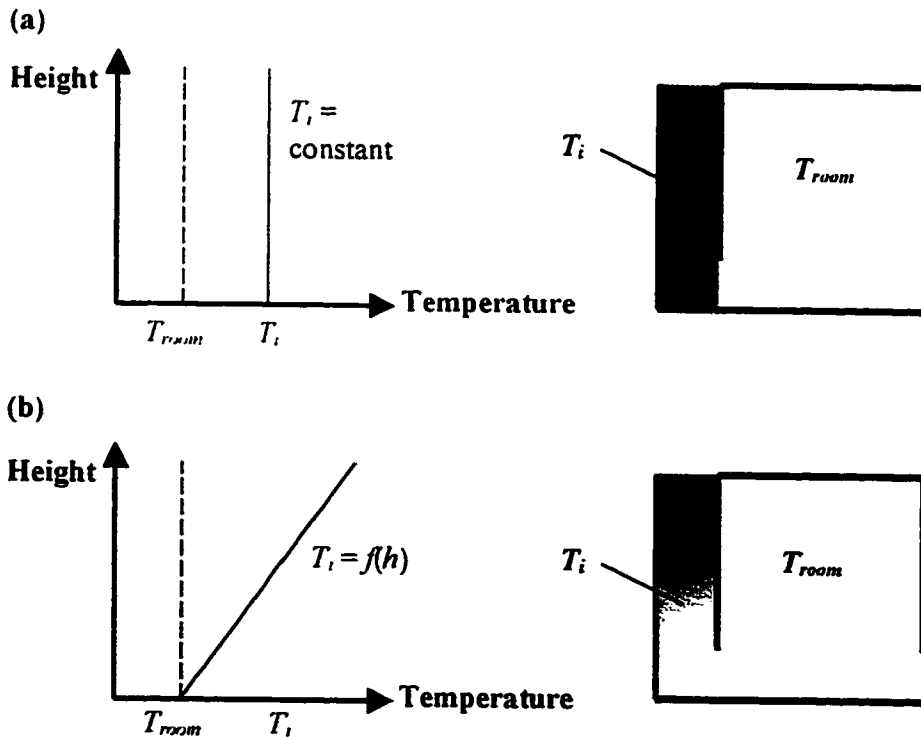
Figure 5.1 Temperature distribution for (a) Model 1 and (b) Model 2.

77

$$\Delta P_s = (\rho_o - \rho_i)gH$$

$$= \rho \frac{\Delta T}{T} gH \tag{5.3}$$

where ΔT is the difference between the inside temperature of the chimney and the outdoor temperature, and ρ is some reference density.

An energy balance on the solar chimney yields:

$$\Delta T = \frac{q}{Q\rho C_p} \tag{5.4}$$

where q is the total heat input into the chimney, Q is the flow rate through the system and C_p is the specific heat of the fluid. Inserting Equation (5.4) into Equation (5.3) yields

$$\Delta P_s = \frac{\rho q g H}{Q\rho C_p T} \tag{5.5}$$

Equation (5.5) may be simplified by noting that the specific buoyancy flux, B, can be expressed as:

$$B = \frac{qg}{\rho C_p T} \tag{5.6}$$

Now, using the above expression for buoyancy flux, Equation (5.5) can be written in terms of B, as follows:

$$\Delta P_s = \frac{\rho B H}{Q} \tag{5.7}$$

The total pressure loss, ΔP_L in the system is equal to the sum of the individual pressure losses:

$$\Delta P_L = \Delta P_{ri} + \Delta P_{ci} + \Delta P_{co} + \Delta P_{sc} \tag{5.8}$$

Individual pressure losses exist at the room inlet (ri). the chimney inlet (ci). the chimney outlet (co), and in the solar chimney itself (sc) due to friction. The total pressure loss in the system can be rewritten as:

$$\Delta P_t = \frac{\rho u_n^2}{2c_n^2} + k_{ci}\frac{\rho u_{ci}^2}{2} + k_{co}\frac{\rho u_{co}^2}{2} + k_f\frac{\rho u_{sc}^2}{2} \tag{5.9}$$

The first term on the right-hand-side of Equation (5.9) deals with pressure losses at the ventilation inlet, where c is the discharge coefficient, and u is the velocity. The second and third terms account for pressure losses at the elbowed chimney inlet and the losses at the chimney exhaust, respectively, where k is the pressure losses coefficient. The last term deals with pressure losses due to friction along the chimney walls, where k_f is the channel loss coefficient. Since velocity can be expressed as $u = Q A$. Equation (5.9) can written:

$$\Delta P_L = \frac{\rho(Q/A_n)^2}{2c_n^2} + k_{ci}\frac{\rho(Q/A_{ci})^2}{2} + k_{co}\frac{\rho(Q/A_{co})^2}{2} + k_f\frac{\rho(Q/A_{sc})^2}{2} \tag{5.10}$$

Now, Equations (5.7) and (5.10) are equated (as specified by Equation (5.1)) and rearranged to obtain the expression for ventilation flow rate, Q:

$$Q_1 = (2BH)^{\frac{1}{3}} A^{*\frac{2}{3}} \tag{5.11}$$

where Q_1 is the predicted flow rate for Model 1 and A^* is the effective opening area of the system. It is noted that the cross-sectional area of the chimney is equal to the chimney outlet area, i.e. $A_{co} = A_{sc}$, thus we have:

$$A^* = \sqrt{\frac{1}{\frac{1}{(c_n A_n)^2} + k_{ci}\frac{1}{A_{ci}^2} + (k_{co} + k_f)\frac{1}{A_{co}^2}}} \tag{5.12}$$

5.2 Linear Temperature Distribution in the Solar Chimney – Model 2

Now the second model is derived; this time assuming a linear temperature

distribution within the solar chimney cavity. The second model is developed in the same

manner as the first, but the density within the chimney decreases linearly with height

(since the temperature increases linearly with height). Therefore, the stack pressure is

expressed by:

$$\Delta P_s = \int_0^H (\rho_a - \rho_h) g dh \tag{5.13}$$

$$= \int_0^H \rho \frac{\Delta T_h}{T} g dh \tag{5.14}$$

where ρ_h is the mean density within the solar chimney at height h and ΔT_h is the

difference between the mean temperature and the ambient temperature at height h.

An energy balance on the solar chimney yields:

$$\Delta T_h = \frac{q_h h}{Q \rho C_p} \tag{5.15}$$

where q_h is the heat flow per unit height. Inserting the above Equation (5.15) for

temperature difference into Equation (5.14) yields:

$$\Delta P_s = \int_0^H \frac{\rho q_h h g}{Q \rho C_p T} dh \tag{5.16}$$

$$= \frac{\rho q_h g H^2}{2 Q \rho C_p T} \tag{5.17}$$

Considering that the specific buoyancy flux, in terms of q_h, is

$$B = \frac{q_h H g}{\rho C_p T} \tag{5.18}$$

the equation for stack pressure becomes

$$\Delta P_s = \frac{\rho BH}{2Q} \tag{5.19}$$

The total pressure loss in the system is the same as that expressed in Equation (5.10). Equating Equations (5.10) and (5.19), and rearranging, we obtain:

$$Q_2 = A_e^{\frac{2}{3}} (BH)^{\frac{1}{3}} \tag{5.20}$$

where Q_2 is the flow rate predicted by Model 2.

A simple observation between Equation (5.11) and Equation (5.20) reveals that

$$Q_1 = \sqrt[3]{2} Q_2 \tag{5.21}$$

Therefore, by assuming a uniform temperature in the solar chimney, the predicted ventilation flow rate is 26% higher than that predicted by a linear temperature distribution assumption.

5.3 Pressure Losses in the Solar Chimney Ventilation System

To solve Equations (5.11) and (5.20), it is necessary to specify the four loss factors given in Equation (5.12).

5.3.1 Pressure Losses at the Ventilation Inlet

When fluid enters a sharp-edged opening, flow separation takes place, resulting in contraction of the entering fluid jet. This is known as the vena contracta. The vena contracta effectively reduces the area of the inlet, therefore reducing the flow rate. The ratio of the cross-sectional area of the vena contracta to that of the opening is known as

the discharge coefficient, c. A relationship also exists between c and the pressure drop across the opening:

$$c = \frac{Q}{A}\sqrt{\frac{\rho}{2\Delta P}} \tag{5.22}$$

Note: if this equation is solved for the total pressure loss, ΔP, an expression for pressure loss across an opening is obtained; this is the form of the first term in Equation (5.10) at the room inlet.

Sharp-edged openings, and the associated discharge coefficient, are of interest in building ventilation design because of their similarity with ventilation components, such as open windows and intake vents. The discharge coefficient for a sharp-edged inlet is typically taken as 0.61. This value remains constant, or at least close to constant, down to Re values of order 100 [27]. At Re numbers lower than this, the discharge coefficient becomes less than 0.6, depending on the Re number [27].

In this work, the discharge coefficient was taken as that for a sharp-edged opening. That is, the discharge coefficient at the room inlet is $c_n = 0.61$.

5.3.2 Pressure Losses at the Chimney Inlet and Exit

It is convenient, especially in ducted flow, to talk of the loss coefficient, k:

$$k = \frac{\Delta P}{(\rho u^2 / 2)} \tag{5.23}$$

where ΔP is the total pressure loss across a length of duct or pipe, or across a given component (eg. an elbow or section change). If Equation (5.23) is solved for ΔP, the form of the last three terms, on the right hand side of Equation (5.10), is obtained. The loss coefficients in the second and third terms refer to local losses at the chimney inlet (k_{ci})

and the chimney exit (k_{co}). The loss coefficient in the last term (k_f) refers to friction losses along the chimney walls, and will be discussed in the next section.

In the present work, the velocity distribution exiting the chimney was asymmetrical because of the unevenly heated chimney channel. Therefore the exit loss coefficient was approximated using a loss coefficient, $k_{co} = 3.67$, as specified by Fried and Idelchik [28].

Data for pressure losses entering the chimney inlet were harder to come by. At first it was considered that a loss coefficient for a 90°-elbow within a duct be used. However, this option was disregarded because information found in published duct design data, such as Fried and Idelchik [28], is appropriate for $Re \geq 10^4$ for ducted elbows. However, Reynolds numbers calculated in the present work were found to be in the range 100 to 1000. Additionally, a ducted elbow does not accurately simulate the geometry of the chimney inlet: the flow enters from the relatively open room into the chimney. For this reason, the loss coefficient at the chimney inlet was approximated as that for fluid entering a straight shaft, giving $k_{ci} = 12.6$ [28]. Note that this value is probably, in most cases, higher than the actual pressure loss that occurred in the experiments. In reality the k values vary with the ratio of chimney inlet area to chimney channel area and the Reynolds number.

It should be noted that a relationship exits between the discharge coefficient (c) and the loss coefficient (k):

$$c = \frac{1}{\sqrt{k}}$$

(5.24)

This relationship is easily obtained from Equations (5.22) and (5.23).

5.3.3 Friction Losses in the Solar Chimney

Friction losses occur within the chimney cavity itself, since the cavity walls slow the fluid down. The channel loss coefficient, k_f, can be used to determine the friction losses within a chimney:

$$k_f = f \frac{H}{D_H} \tag{5.25}$$

where f is the friction factor, H is the height of the chimney, and D_H is the hydraulic diameter. The hydraulic diameter, for a rectangular solar chimney, can be found by:

$$D_H = \frac{2wd}{w + d} \tag{5.26}$$

where w is the width and d is the depth of the solar chimney.

For laminar flow, the friction factor (f) depends only on the Reynolds number, and can be calculated by the following equation:

$$f = \frac{64}{Re_{D_H}} \tag{5.27}$$

For transitional and turbulent flow, f depends on the Reynolds number and the surface roughness of the chimney walls (ε). In this case, the friction factor can be calculated conveniently from the Altshul-Tsal equation [24]:

$$f' = 0.11 \left(\frac{\varepsilon}{D_H} + \frac{68}{Re_{D_H}} \right)^{0.25}$$

If $f' \geq 0.018$: $\quad f = f'$

If $f' < 0.018$: $\quad f = 0.85 f' + 0.0028$

$$\tag{5.28}$$

The Reynolds number based on hydraulic diameter (Re_{D_H}) is given by

$$Re_{c} = \frac{D_{H} u}{\nu} \qquad (5.29)$$

As mentioned above, low values of Reynolds number were found in the experiments. However, as indicated by the Rayleigh number (see Section 3.3) and from experimental observations, the fluid flow, at least in the plume, was clearly turbulent. The low Reynolds numbers predicted may be due to low velocities experienced away from the plume, near the unheated wall of the chimney, hence giving a low average velocity in the chimney. Consequently, the friction loss within the channel was then approximated using the friction factor described in Equation (5.27).

5.4 Analysis of Experimental and Theoretical Results

Comparisons between theoretical and experimental results are shown in Figures 5.2 to 5.6. It can be clearly seen that the analytical models generally over-predict the ventilation flow rate. The large discrepancy between the predictions and the experimental results could be due to three main factors: simplified temperature assumptions within the solar chimney channel, incorrect values of specified loss coefficients and the presence of backflow in the chimney at large chimney widths.
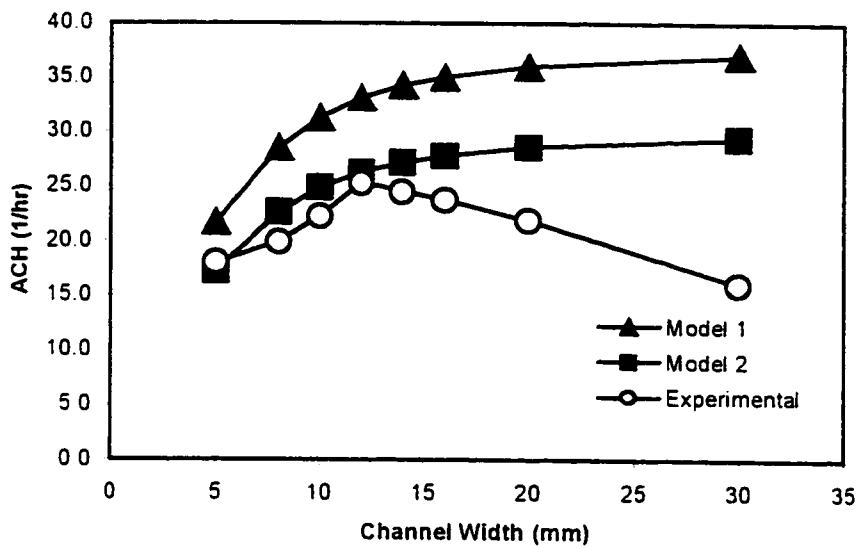
Figure 5.2 Comparison between experimental and analytical results at Mode (I)

and $B = 489\text{cm}^4/\text{s}^3$.
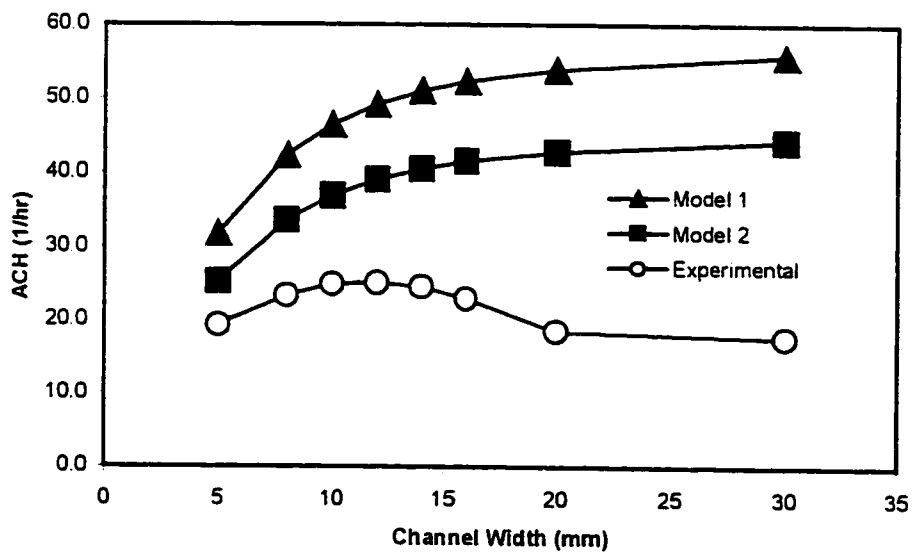
Figure 5.3 Comparison between experimental and analytical results at Mode (II)

and $B = 367\text{cm}^4/\text{s}^3$.
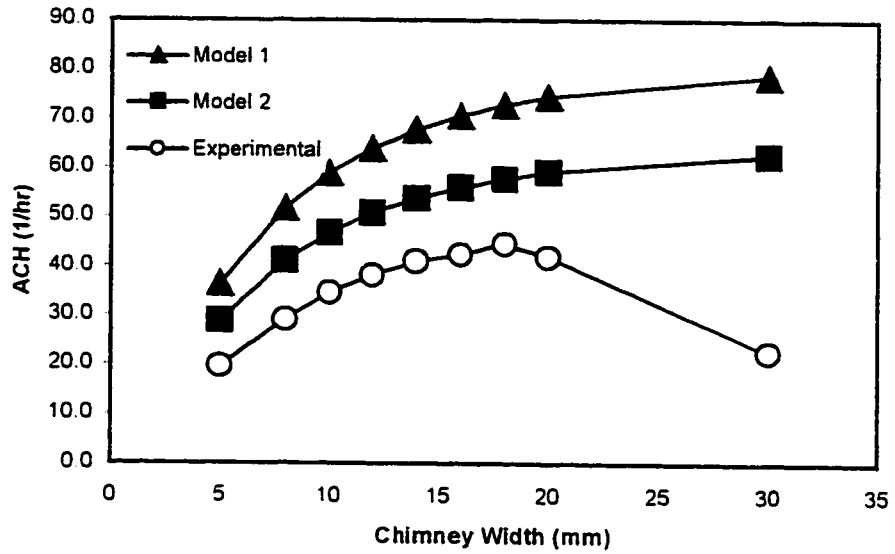
Figure 5.4 Comparison between experimental and analytical results at Mode (III)

and $B = 489 \text{cm}^4/\text{s}^3$.
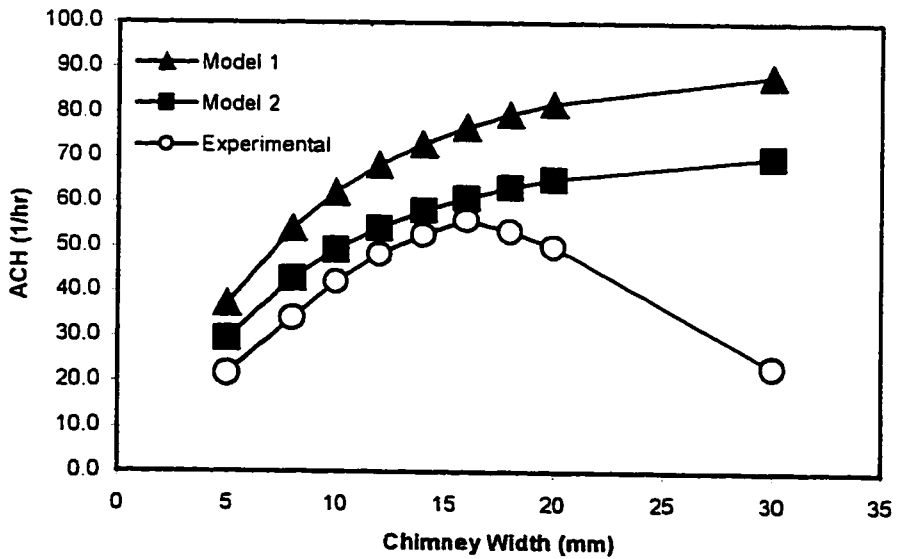
Figure 5.5 Comparison between experimental and analytical results at Mode (IV)

and $B = 489 \text{cm}^4/\text{s}^3$.
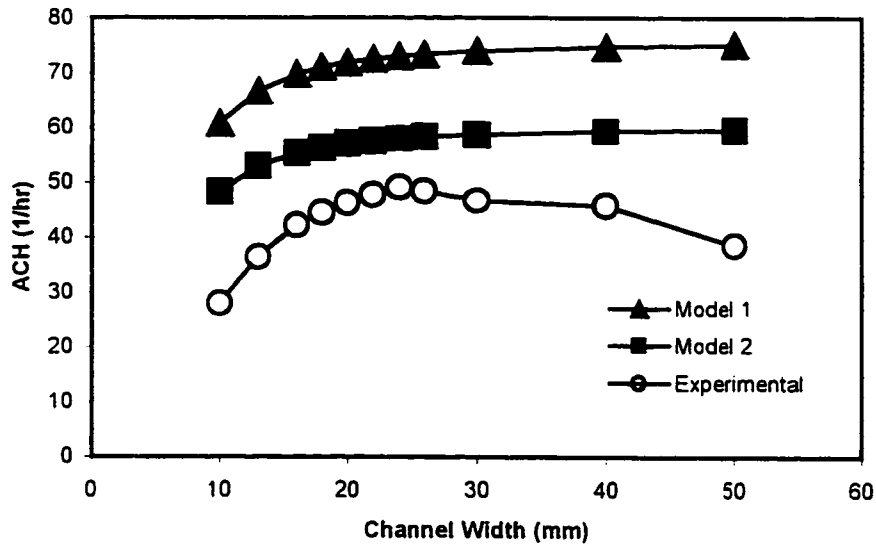
Figure 5.6 Comparison between experimental and analytical for the 400mm high chimney at Mode (I) and $B = 489\text{cm}^4/\text{s}^3$.

In both models, the temperature distribution is significantly different from reality. Model 1 assumes a constant temperature throughout the chimney while Model 2 assumes a linear temperature distribution in the chimney. In both cases, the temperature is assumed constant across the width of the chimney at a given height. In reality, the temperature distribution looks more like that shown in Figure 5.7. As a result, the uneven temperature distribution across the width of the channel may result in smaller stack pressure and ventilation rates compared with predicted values. In all cases, Model 1 grossly over-predicted the ventilation flow rate, suggesting that a uniform temperature assumption within the chimney is much too simplified for the purpose of solar chimney ventilation prediction.
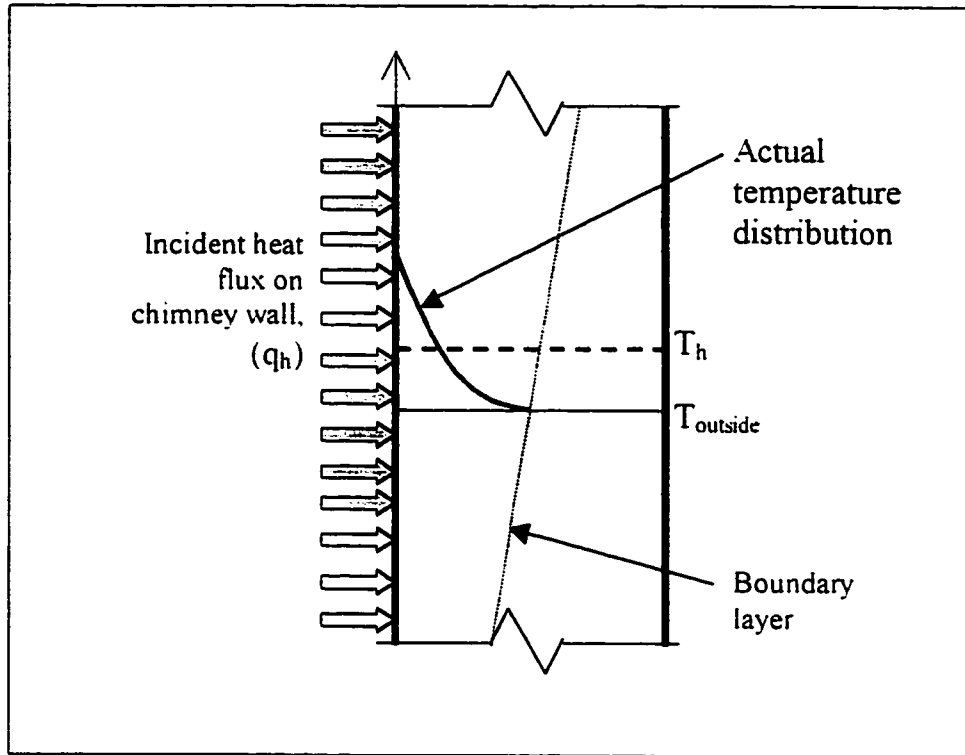
Figure 5.7 Assumed and actual temperature distribution in the solar chimney

It can be seen that for Modes (III) and (IV) (see Figures 5.4 and 5.5) theoretical

predictions are in closer agreement with experimental values than for Modes (I) and (II)

(see Figures 5.2 and 5.3). This is probably due to increased mixing of the bubble plume

for larger chimney inlet areas as observed during the experiments. As discussed in the

previous chapter, the mixing effect distributed the temperature more evenly across the

chimney. Hence, at Modes (III) and (IV), the temperature distribution in the channel

more closely approached the theoretical assumptions, giving better agreement between

the theoretical predictions and the experimental results.

Another explanation for over-prediction by the theoretical analysis could be

incorrect assignment of pressure loss values, especially at the chimney inlet and exit

(represented by k_{ci} and k_{co}). Here, there is limited information on universal pressure loss

coefficients, and this is made more evident by the general disagreement in literature as to

which values to use. Certainly, more research must be done in this area if a simple analytical prediction tool is to be successfully implemented.

The theoretical models considered do not have the ability to predict backflow within the solar chimney. However, the simple models may still be useful for predicting flow rates up to the optimum chimney width. For example, referring to Figure 5.5, it can be seen that the curve of Model 2 closely follows the experimental measurements up to the optimum chimney width. However, after this point the difference between the two curves increases as the chimney is widened.

CHAPTER 6

CONCLUSION

6.1 Summary of Results

The aim of this work was to study the natural ventilation performance of a solar chimney system. It is evident from literature that there is limited understanding of solar chimney ventilation, due mostly to the complex turbulent flow behaviour within the vertical chimney channel. Such barriers on understanding must be overcome if solar chimney ventilation systems are to be designed and operated effectively. Considering this, a small-scale solar chimney model was developed so important parameters of solar chimney height and width, ventilation inlet area, and radiant heat flux incident upon a chimney wall could be experimentally investigated.

A fine-bubble modelling technique was used for the investigation. A plume of fine hydrogen bubbles was generated along a wall of the solar chimney producing density differences within the chimney, thus simulating temperature differences caused by heating a single wall of the solar chimney with a constant heat flux.

The small-scale solar chimney model used in this experiment repeated a number of important phenomena previously reported by other researchers. For example, it was found that an optimum chimney width occurred giving maximum ventilation performance. Additionally, experiments with different solar radiation intensity showed that the optimum chimney width was independent of source strength, but became larger for large chimney inlets.

As expected, the experiments showed that the ventilation flow rate increased with an increase in ventilation inlet area. It was found that, at moderate to large chimney widths, the effect of chimney inlet area on the ventilation flow rate was more significant than the effect of room inlet area. This was due to increased pressure losses at the chimney inlet compared to the room inlet; consequently, increasing the chimney inlet reduced the total pressure loss through the system more than increasing the room inlet. However, at small chimney widths, friction losses in the solar chimney became more critical in reducing the flow rate.

Results showed that the optimum chimney width increased with chimney height, and did so linearly, such that the optimum aspect ratio (chimney height: optimum chimney width) remained constant. If indeed the optimum chimney width is an indication of the boundary layer thickness, then it appears that the boundary layer varies linearly along the height of the uniformly heated chimney wall.

Furthermore, when the chimney height was doubled, the maximum ventilation flow rate doubled. Such a result indicates that increasing chimney height can be effective in increasing the ventilation flow rate.

In addition to the experiments, two simple analytical models were developed based on common solar chimney ventilation predication tools found in literature: (1) a model based on a uniform temperature in the chimney, and (2) a model based on linear temperature distribution in the chimney. When compared to the experimental results, it was found that the theoretical models generally over predicted the ventilation flow rate. Possible reasons for the discrepancy may be due to three main factors: incorrect temperature assumptions in the chimney channel; incorrect pressure loss assumptions for

friction along the chimney and at the ventilation openings; and the inability of the analytical models to predict backflow in the chimney.

Simplified temperature assumptions are a very likely cause of over prediction by the analytical models; this is especially true of Model 1, indicating that a uniform temperature distribution within the chimney should not be assumed when designing a solar chimney ventilation system. Model 2 correlated somewhat better to the experimental data, especially at larger chimney inlets when the bubble plume was dispersed and created a more even temperature distribution in the channel.

One way the analytical models could fit the experimental data (up to the optimum width) more precisely would be if the total pressure loss through the system was greater than that assumed. However, general information that exists in literature on pressure loss coefficients is mostly for duct and pipe design, where the flow is assumed to possess a uniform velocity profile. As a result such information is inadequate for the geometries and complex flow behavior that exists in solar chimney ventilation systems. Specifically, entrance losses for the chimney inlet geometry, and chimney friction and exit losses for a non-uniform velocity profile needs further investigation.

The two simple analytical models failed to predict backflow in the solar chimney, but this was expected: boundary layer flow needs to be considered if backflow is to be predicted. However, simple analytical models, such as the ones investigated in the current work, can still be useful to designers if they can accurately predict the ventilation flow rate up to the optimum chimney width before backflow occurs.

6.2 Design Considerations

The results of this work have provided some important implications for solar chimney designers. The solar chimney can be designed for an optimum chimney width, which will remain constant with variation of solar radiation intensity. The optimum chimney width should be designed based on boundary layer thickness at the top of the channel and pressure losses, especially at the chimney inlet.

In addition to designing a solar chimney for optimum width, other effective ways to naturally induce acceptable flow rates are to specify tall solar chimneys and/or large ventilation inlet areas. Furthermore, increasing the chimney inlet area is more effective in providing ventilation than increasing the room inlet area. This is true up to a certain limit, however, as increasing the chimney inlet decreases the effective stack height and reduces the amount of wall area for storing heat.

Unfortunately, the present work has not identified a consistently accurate yet simple prediction tool for solar chimney ventilation; rather, it has exposed weakness of current models in literature and has identified some important difficulties that must be overcome in order to develop an effective prediction tool. Results indicate that a uniform temperature distribution within the chimney is too simplified an assumption to be applied to solar chimney ventilation for mathematical prediction. Additionally, this nullifies the use of numerous zonal-model computer programs, used for airflow prediction and analysis, for the purpose of solar chimney ventilation.

6.3 Topics for Future Research

The results have left a number of things investigated inconclusive, indicating topics for future research. For example, very little work has been done on turbulent natural convection heat transfer and fluid flow in a heated vertical channel. More research could be done in this area, especially investigating airflow rate and backflow effects.

More research on pressure loss coefficients for solar chimney building geometries should be done. This information would be useful for designers using simple theoretical models to predict the ventilation flow rate through the building.

It would be useful to perform a CFD or numerical analysis to compare to the experiments. This would also be another way to obtain pressure loss coefficients for the situations studied in the experiments.

Further tests could be undertaken to validate the buoyancy flux produced by the fine-bubble technique used in this experiment. Existing literature on the fine-bubble technique has only validated the height of stratification layers in buildings using displacement ventilation.

REFERENCES

1. Di Cristofalo, S., Orioli, S., Silvestrini, G., Alessandro, S., Thermal Behavior of "Scirocco Rooms" in Ancient Sicilian Villas. *Tunnelling and Underground Space Technology*, 1989, 4(4) 471-473.

2. Bouchair, A., Solar Chimney for Promoting Cooling Ventilation in Southern Algeria. *Building Serv. Eng. Res. Technol.*, 1994, 15(2), 81-93.

3. Barozzi, G. S., Imbabi, M. S. E., Nobile, E., Sousa, A. C. M., Physical and Numerical Modelling of a Solar Chimney-based Ventilation System for Buildings. *Building and Environment*, 1992, 27(4), 433-445.

4. Bansal, N. K., Mathur, R., Bhandari, M. S., Solar Chimney for Enhanced Stack Ventilation. *Building and Environment*, 1993, 28(3), 373-377.

5. Bansal, N. K., Mathur, R., Bhandari, M. S., A Study of Solar Chimney Assisted Wind Tower System for Natural Ventilation in Buildings. *Building and Environment*, 1994, 29(4), 495-500.

6. Gan, G., A Parametric Study of Trombe walls for Passive Cooling of Buildings. *Energy and Buildings*, 1998, 27, 37-43.

7. Lane-Serff, G. F., Linden, P. F., Parker, D. J., Smeed, D. A., Laboratory Modelling of Natural Ventilation Via Chimneys. Proceedings of the 9th international PLEA conference: Architecture and Space, Seville, Spain, 1991. Edited by Alvarez, S., Lopez de Asain, J., Yannas, S., Fernandes, O. 505 – 510.

8. Kumar, S., Sinha, S., Kumar, N., Experimental Investigation of Solar Chimney Assisted Bioclimatic Architecture. *Energy Convers. Mgmt.*, 1998, 39(5/6), 441 - 444.

9. Khedari, J., Boonsri, B., Hirunlabh, J., Ventilation Impact of a Solar Chimney on Indoor Temperature Fluctuation and Air Change in a School Building. *Energy and Buildings*, 2000, 32, 89 – 93.

10. Afonso, C., Oliveira, A., Solar Chimneys: Simulation and Experiment. *Energy and Buildings*, 2000, 32, 71 – 79.

11. Sandberg, M., Moshfegh, B., Investigation of Fluid Flow and Heat Transfer in a Vertical Channel Heated From One Side by PV Elements: Part II – Experimental Study. *WREC*, 1996, 254 – 258.

12. Sandberg, M., Moshfegh, B., Ventilated Solar Roof Air Flow and Heat Transfer Investigation. *Renewable Energy*, 1998, 15, 287-292.

13. Moshfegh, B., Sandberg, M., Flow and Heat Transfer in the Air Gap Behind Photovoltaic Panels. *Rewnewable and Sustainable Energy Reviews,* 1998, 2, 287-301.

14. Swainson, M. J., Evaluation of the potential of solar chimneys to drive natural ventilation in non-domestic buildings, Ph.D. Thesis, Cranfield University, UK, 1997.

15. Eckert, E and Jackson, T., Analysis of Turbulent Free-convection Boundary Layer on a Flat Plate. Report 1015, NACA, Washington DC, 1951.

16. Hamdy, I. F. and Firky, M. A., Passive Solar Ventilation. *Renewable Energy,* 1998, 14(1-4), 381-386.

17. Awbi, H. B., Design Considerations for Naturally Ventilated Buildings. *Renewable Energy,* 1994, 5, Part II, 1081 – 1090.

18. Padki, M. M. and Sherif, S. A., On a Simple Analytical Model for Solar Chimneys. *Int. J. Energy Res.,* 1999, 23, 345-349.

19. Bouchair, A. Solar Induced Ventilation in the Algerian and Similar Climates, PhD Thesis, University of Leeds, UK, 1989.

20. Gan, G., Riffat, S. B., A Numerical Study of Solar Chimney for Natural Ventilation of Buildings with Heat Recovery. *Applied Thermal Engineering*, 1998, **18**, 1171-1187.

21. Akbari, H. and Borgers, T. R., Free Convective Flow within the Trombe Wall Channel. *Solar Energy*, 1979, **22**, 165-174.

22. Borgers, T. R. and Akbari, H., Free Convective Turbulent Flow within the Trombe Wall Channel. *Solar Energy*, 1984, **33(3/4)**, 253-264.

23. Tichy, J. A., The Effect of Inlet and Exit Losses on Free Convection Laminar Flow in the Trombe Wall Channel. *Journal of Solar Energy Engineering*, 1983, **105**, 187-93.

24. ASHRAE Handbook of Fundamentals, American Society of Heating Refrigeration and Air-conditioning Engineers Inc., Atlanta, GA, 1989, pp 32.21-32.46.

25. Chen, Z. D., Li, Y., Mahoney, J., Experimental Modelling of Buoyancy-Driven Flows in Buildings Using a Fine-Bubble Technique. Prepared for *Building and Environment*, 1999.

26. Chen, Z. D., Li, Y., Mahoney, J., Natural Ventilation in an Enclosure Induced by a Heat Source Distributed Over a Vertical Wall. Prepared for *Building and Environment*, 1999.

27. Etheridge, D.W. and Sandberg, M., Building Ventilation: Theory and Measurement, John Wiley & Sons Ltd, 1996, pp. 90-91, 206-209, 649-667.

28. Fried, E. and Idelchik, I. Flow Resistance, a Design Guide for Engineers, Hemisphere Publishing Corp., New York, 1989.

APPENDIX A

CALCULATION OF BUOYANCY FLUX

The buoyancy flux can be calculated by

$$B = gQ_g \frac{(\rho_s - \rho_g)}{\rho_s} \tag{3.1}$$

where the hydrogen bubble gas flow rate (Q_g) may be calculated from

$$Q_g = \frac{V}{nF} It$$

where

g = acceleration due to gravity

ρ_s = density of the salt-water solution

ρ_g = density of hydrogen gas

V = 24.05 litre/mol, the volume per mole of gas at 20°C

I = current

t = time (s)

n = valence of the material (for hydrogen $n = 2$)

F = 96 485.309 C/mol is the Faraday's constant

Example

For I = 1A and t = 1s, the hydrogen gas flow rate at 20°C is calculated as

$$Q_g = (24.05\text{L/mol} \times 1\text{A} \times 1\text{s})/(2 \times 96485.309\text{C/mol})$$

$$= 1.246 \times 10^{-4} \text{ L/s}$$

Note: 1A = 1C/s

101

Since $\rho_s \gg \rho_g$, Equation (3.1) may be written

$$B = gQ_g \frac{\rho_s}{\rho_s} = gQ_g$$

thus

$$B = 9.81\,\text{m/s}^2 \times 1.246 \times 10^{-4}\text{L/s} \times 1\text{m}^3/1000\text{L} \times 10^8\text{cm}^4/1\text{m}^4$$

$$= 122\ \text{cm}^4/\text{s}^3$$

APPENDIX B

CALCULATION OF ERROR DUE TO THE DISINTEGRATION OF CATHODE WIRES

At times during the experiments there would be one or two cathode wires that would start to disintegrate. This was probably due to current flowing from one section of the cathode to another. In the worst case, it was found that two wires were completely disintegrated after approximately three hours, at a buoyancy flux of 489 cm^4/s^3. The maximum error induced by the disintegration will be subsequently detailed.

The total volume of the wires is

$$V = \pi \left(\frac{d}{2}\right)^2 Ln$$

where

d = 0.5mm, diameter of wire

L = 100mm, length of wire

n = 2, number of wires

This yields

$$V = 3.92699 \times 10^{-8} \text{ m}^3$$

The mass flow rate is calculated from

$$\dot{m} = \frac{\rho_c V}{t}$$

where

ρ_c = 9.8 × 10^6 g/m^3, the density of copper

t = 3hr, the time is takes for the wire to fully dissolve

This yields

$$\dot{m} = 0.12828 \text{g/hr}$$

Since one mole of copper is 63.55g, the equivalent mass flow rate for H_2 gas due to the disintegration of the copper wires is

$$\dot{m} = 2.01859 \times 10^{-3} \text{ mol/hr}$$

$$= 0.04844 \text{ L/hr (since 24.05 is the volume per mole of gas at 20°C)}$$

Therefore, a maximum of 0.04844 L/h of gas is not being produced due to the disintegration of the copper wires. At a buoyancy flux of 489 cm^4/s^3, with all wires working, the gas flow rate is 1.795 L/hr. Consequently, the maximum error is

$$\text{error} = (0.04844/1.795) \times 100$$

$$= 2.7\%$$

APPENDIX C

REPEATABILITY ANALYSIS

To test the repeatability of the experimental technique several retrials were performed. Results of the tests are shown in the figures below. Retrials were performed at Modes (I), (II) and (III) at a buoyancy flux $367 cm^4/s^3$.

It was found that for Mode (I) the average deviation from the mean value in the velocity measurement was $\pm 5\%$ and the maximum deviation was about $\pm 10\%$. Similarly, for Mode (II) the average and maximum deviations were $\pm 2.1\%$ and $\pm 3.9\%$ respectively and for mode (III) the average and maximum deviations were $\pm 2.9\%$ and $\pm 6.4\%$ respectively. The large deviation encountered in Mode (I) may be because different sets of cathodes were used for the repeated experiments. The difference in the deterioration and the distance between wires of the two cathodes used in the tests probably contributed to the deviations. It should be noted that data for the 5mm chimney width was not included in the repeatability analysis. The reason for this is that flow conditions at the 5mm width were at times dependent on the initial conditions in the chimney. That is, when the power supply was turned on, it was observed that, at times, bubbles formed at a faster rate in some parts of the chimney than others, causing bubbles to get trapped at the narrow chimney width. The influence of trapped gas bubbles was only observed for the narrow 5mm chimney width.